A NOVEL INTERVAL FINITE ELEMENT METHOD BASED ON THE IMPROVED INTERVAL ANALYSIS

Alba Sofi[1,*], Eugenia Romeo[2]

[1]Department of Architecture and Territory and Inter-University Centre of Theoretical and Experimental Dynamics, University "Mediterranea" of Reggio Calabria, Salita Melissari, Feo di Vito, 89124 Reggio Calabria, Italy. E-mail: alba.sofi@unirc.it

[2]Department of Civil, Energy, Environmental and Materials Engineering, University "Mediterranea" of Reggio Calabria, Via Graziella, Località Feo di Vito, 89124 Reggio Calabria, Italy. E-mail: eugenia.romeo@unirc.it

Abstract

Static analysis of linear-elastic structures with uncertain parameters subjected to deterministic loads is addressed. The uncertain structural properties are modeled as interval variables with assigned lower bound and upper bound. A novel Interval Finite Element Method is formulated in the framework of the *improved interval analysis via extra unitary interval*, recently proposed to limit the conservatism affecting the *classical interval analysis*. The key idea of the novel method is to associate an *extra unitary interval* to each uncertain parameter in order to keep physical properties linked to the finite elements in both the assembly and solution phases. This allows one to reduce overestimation and perform standard assembly of the interval element matrices. The lower bound and upper bound of interval displacements and stresses are evaluated by applying two different strategies both based on the so-called *Interval Rational Series Expansion* for deriving the approximate explicit inverse of the interval global stiffness matrix. Numerical examples concerning 2D and 3D structures with uncertain Young's modulus are presented to demonstrate the accuracy and efficiency of the proposed procedure.

Keywords: interval uncertainties, finite element method, improved interval analysis, extra unitary interval, Interval Rational Series Expansion, lower bound and upper bound.

*Corresponding author

1. INTRODUCTION

In practical engineering, the actual values of design parameters are always affected by some degree of uncertainty [1]. The ability to incorporate non-deterministic properties in numerical modeling is of great importance in order to allow realistic reliability assessment of engineering systems. Traditionally, probability theory is used to handle uncertainties affecting design parameters. Recently, criticism has arisen on the applicability of probabilistic approaches when available data are insufficient to define the probability density function (PDF) of the uncertain properties or when information is ambiguous, vague or imprecise [2]. In such situations, uncertainties can be quantified and processed using alternative approaches based on non-probabilistic concepts, such as convex models, interval model, fuzzy-set theory, etc. [3-6]. The interval model, originally developed from the *classical interval analysis* (*CIA*) [7,8], represents the uncertain parameters as interval variables with given lower bound (LB) and upper bound (UB). This model turns out to be a suitable tool when the range of variability of the uncertain parameters is known, while available information is insufficient to define the type of distribution within such range.

Since the mid-1990s, the interval model of uncertainty has been applied in the context of finite element analysis giving rise to the so-called Interval Finite Element Method (IFEM). Several versions of the method have been developed with the purpose of finding sharp bounds of the solution. Most research in this area starts from the interval global equilibrium equations and focuses entirely on the approximation of the solution set, ignoring the shortcomings inherent in the assembly phase [2]. Rao and Berke [9] used a computationally intensive combinatorial approach to evaluate the bounds of the interval response. Many researchers developed perturbation-based approaches (see e.g. [10,11]) whose applicability is restricted to small widths of the uncertain parameters. McWilliam [12] proposed two methods to compute the bounds of structural response: a modified version of interval perturbation analysis and a procedure based on the assumption that the displacement surface is monotonic. Comparisons between the results of stochastic and interval finite element analysis have also been performed [13,14]. Relying on the assumption of monotonic system output, Pownuk [15] proposed a sensitivity analysis method which gives a very good inner approximation of the exact solution set. For a general overview of the state-of-art and recent advances in interval finite element analysis, readers are referred to [2,16].

The main challenge faced by researchers since the first development of the IFEM was the reduction of the overestimation of the interval solution range due to the so-called *dependency phenomenon* [7] which introduces conservatism not only in the solution phase, but also in the assembly of the system matrices [2]. The reason behind this phenomenon is the inability of the *CIA* to recognize multiple occurrences of the same interval variable which actually has a physical meaning in the context of the IFEM. The amount of overestimation increases with the width of interval uncertainties and the problem size often leading to totally useless results. To eliminate many sources of overestimation in interval-based finite element analysis, Muhanna and Mullen [17] developed the element-by-element (EBE) technique in which elements are kept disassembled and the Lagrange multiplier method is applied to ensure compatibility and equilibrium. Neumaier and Pownuk [18] proposed a method to compute accurate bounds of the displacements for high-dimensional problems with large uncertainties, but applications are restricted to truss structures.

In the literature, several improvements of the *CIA* have been introduced to limit conservatism such as: the *affine arithmetic* (*AA*) [19], the *parameterized interval analysis* (*PIA*) [20] and the *improved interval analysis via extra unitary interval* (*IIA via EUI*) [21]. Recently, an improvement of interval finite element analysis based on the *AA* has been proposed by Degrauwe *et al.* [22]. The *PIA* and the *IIA via EUI* have been specifically developed to perform interval structural analysis by taking into account dependencies between interval variables which actually represent physical properties of the structure. To this aim, the *IIA via EUI* introduces a particular unitary interval, the so-called *EUI*, which is associated to each interval variable and does not follow the rules of the *CIA*. A combination of the *PIA* and the *IIA via EUI* has been presented in [23].

Another challenging issue to be faced in the context of interval-based finite element computations is to obtain sharp bounds of the secondary variables (stress) which suffer from additional overestimation with respect to the primary variables (displacements) [24]. To cope with this problem, various extensions of the EBE technique have been presented [25,26]. A significant reduction of the overestimation affecting the bounds of the axial forces in structures with interval axial stiffness has been achieved by Impollonia and Muscolino [27].

Further, a limitation of the interval model lies in the intrinsic inability of the interval variables to represent the spatial variability of uncertainties. As known, assuming independent interval variables for each FE increases both the degree of variability of parameters and the computational effort. Current researches focus on the development of more realistic models of spatially variable interval uncertainties as continuous fields (see e.g. [28-31]). In particular, Moens *et al.* [28] first introduced the concept of *interval field*, recently extended by Muscolino *et al.* [29] in the context of the *IIA via EUI*.

Though significant improvement in the field of interval-based finite element analysis has been achieved so far, in the authors' opinion much research effort is still needed to efficiently deal with problems of engineering interest as well as to obtain reliable predictions of interval stresses, especially when large uncertainties are involved.

The aim of the present study is to develop a novel IFEM able to provide accurate estimates of the bounds of both displacements and stresses for general structures (2D and 3D) with a large number of uncertain parameters even in the presence of relatively high degrees of uncertainty. Without loss of generality, attention is focused on structures made of linear-elastic isotropic material with uncertain Young's modulus. In particular, Young's moduli of selected subdomains, which may coincide or not with the FEs of the adopted mesh, are modeled as independent interval variables. The key idea of the proposed method is to handle interval variables by means of the *IIA via EUI* so that an *EUI* is associated to each uncertain parameter. Practically, the *EUI* links the uncertain physical property to the pertinent FE. This allows one to keep track of the dependencies between interval uncertainties both in the assembly and solution stages of the FE procedure and thus reduce overestimation due to the *dependency phenomenon*. The interval global equilibrium equations of the FE modeled structure can be therefore obtained via standard assembly procedure. In order to evaluate the LB and UB of the interval response, an approximate explicit expression of the inverse of the interval global stiffness matrix of the structure is derived by means of the so-called *Interval Rational Series Expansion* (*IRSE*) [32-35]. The application of the *IRSE* first requires to express the interval stiffness matrix as sum of the nominal value plus an interval deviation given by a superposition of rank-one matrices. To enhance the computational efficiency of the *IRSE* within the FE context, in the present paper this task is accomplished by applying the spectral decomposition of the nominal stiffness matrix of the generic FE. Then, based on the knowledge of the approximate explicit inverse of the interval global stiffness matrix provided by the *IRSE*, two different approaches for evaluating the bounds of the interval displacements and stresses are proposed: the first one exploits the *affine form* expression of the *IRSE* truncated to first-order terms; the second strategy relies on the monotonic behavior of the solution which is predicted by studying the sign of response sensitivities with respect to the uncertain parameters.

The paper is organized as follows: in Section 2, the fundamentals of the *IIA via EUI* are briefly summarized; Section 3 is devoted to the formulation of the novel IFEM based on the use of the *IIA via EUI* and the *IRSE*; in Sections 4 and 5, two different approaches for evaluating the bounds of the interval displacements and stresses are presented; Section 6 briefly describes the formulation of the method when regions larger than the single FE are assumed to exhibit independent variations of the interval Young's moduli; finally, in Section 7, numerical applications are provided to demonstrate the accuracy and efficiency of the proposed method.

2. IMPROVED INTERVAL ANALYSIS VIA EXTRA UNITARY INTERVAL

The interval model is a widely used non-probabilistic approach for handling uncertainties occurring in engineering problems. This model, originally developed from the *interval analysis* [7,8], describes the generic uncertain parameter as an interval variable with given lower bound (LB) and upper bound (UB). No information is given on the probability of occurrence of values between the LB and UB.

Let $\mathbb{IR}$ be the set of all real interval numbers and $\alpha_i^I = [\underline{\alpha}_i, \overline{\alpha}_i] \in \mathbb{IR}$ an interval variable such that $\underline{\alpha}_i \le \alpha_i \le \overline{\alpha}_i$. The symbols $\underline{\alpha}_i$ and $\overline{\alpha}_i$ denote the LB and UB of the interval, respectively, while the apex I characterizes the interval variables. According to the *classical interval analysis* (*CIA*), the *i*-th real interval variable $\alpha_i^I = [\underline{\alpha}_i, \overline{\alpha}_i]$ is characterized by the midpoint value (or mean), $\alpha_{0,i}$, and the deviation amplitude (or radius), $\Delta\alpha_i$, given by:

$$\alpha_{0,i} = \mathrm{mid}\left\{\alpha_i^I\right\} = \frac{\underline{\alpha}_i + \overline{\alpha}_i}{2}; \qquad \Delta\alpha_i = \frac{\overline{\alpha}_i - \underline{\alpha}_i}{2} \tag{1a,b}$$

where $\mathrm{mid}\{\bullet\}$ is an operator yielding the midpoint of the interval quantity between curly brackets.

In the context of engineering applications, the main drawback of the *CIA* is the overestimation of the interval solution due to the so-called *dependency phenomenon* which often leads to useless results for design purpose. This phenomenon occurs when an expression contains multiple instances of one or more interval variables and stems from the inability of the *CIA* to keep track of the dependency between interval variables throughout calculations. To limit the conservatism due to the *dependency phenomenon*, recently the *improved interval analysis via extra unitary interval* (*IIA via EUI*) has been proposed [21]. This approach relies on the introduction of the so-called *EUI*, $\hat{e}_i^I = [-1, +1]$, which is different from the *classical unitary interval* (*CUI*), $e^I = [-1, +1]$, since it does not follow the rules of the *CIA* [21].

The *IIA via EUI* assumes the following *affine form* definition for the i-th interval variable α_i^I:

$$\alpha_i^I = \alpha_{0,i} + \Delta\alpha_i \hat{e}_i^I . \tag{2}$$

It is worth emphasizing that the subscript i means that the *EUI*, $\hat{e}_i^I$, is associated to the i-th interval variable. By associating a different *EUI* to each interval variable, dependencies can be duly taken into account throughout calculations and the overestimation due to the *dependency phenomenon* can be drastically limited.

In the framework of interval symbolism, a generic interval-valued function f and a generic interval-valued matrix function $\mathbf{A}$ of the interval vector $\boldsymbol{\alpha}^I$ will be denoted in equivalent form, respectively, as:

$$\begin{aligned} f^I &\equiv f(\boldsymbol{\alpha}^I) \Leftrightarrow f(\boldsymbol{\alpha}), \quad \boldsymbol{\alpha} \in \boldsymbol{\alpha}^I = [\underline{\boldsymbol{\alpha}}, \overline{\boldsymbol{\alpha}}]; \\ \mathbf{A}^I &\equiv \mathbf{A}(\boldsymbol{\alpha}^I) \Leftrightarrow \mathbf{A}(\boldsymbol{\alpha}), \quad \boldsymbol{\alpha} \in \boldsymbol{\alpha}^I = [\underline{\boldsymbol{\alpha}}, \overline{\boldsymbol{\alpha}}]. \end{aligned} \tag{3a,b}$$

3. NOVEL INTERVAL FINITE ELEMENT METHOD

3.1 Formulation of the interval global equilibrium equations

Let us consider a continuous body made of linear-elastic isotropic material which occupies the volume V bounded by the surface S in its undeformed state. The body is subjected to volume forces $\mathbf{b}(\mathbf{x})$ in V and surface forces $\mathbf{t}(\mathbf{x})$ on the loaded (or free) portion S_t of the boundary surface S, with $\mathbf{x} = [x_1 \quad x_2 \quad x_3]^{\mathrm{T}}$ denoting the position vector of a generic point referred to a Cartesian coordinate system $O(x_1, x_2, x_3)$; the displacements $\tilde{\mathbf{u}}(\mathbf{x})$ are imposed on the constrained portion S_u of S. The loads act by hypothesis in a quasi-static manner and infinitesimal displacements are considered. Without loss of generality, all input parameters are assumed to be known deterministically, except Young's modulus of the material which is treated as an uncertain parameter in the context of the interval model of uncertainty.

Let the volume V of the body be subdivided into N_e finite elements (FEs). As customary in IFEM formulations, Young's modulus of each FE is modeled as an interval variable, i.e.:

$$E^{(i)}(\alpha_i^I) = E_0^{(i)}\left(1+\alpha_i^I\right), \qquad (i = 1, 2, \ldots, N^{(e)}) \tag{4}$$

where $\alpha_i^I = [\underline{\alpha}, \overline{\alpha}] \in \mathbb{IR}$ is the dimensionless fluctuation around the nominal value $E_0^{(i)}$, represented by a symmetric interval variable, i.e. characterized by a zero midpoint value $\alpha_{0,i} = 0$. Following the *IIA via EUI* (see Eq. (2)), the dimensionless fluctuation α_i^I is herein expressed as:

$$\alpha_i^I = \Delta\alpha_i \hat{e}_i^I \tag{5}$$

where $\hat{e}_i^I = [-1, +1]$ is the *EUI* defined in the previous section. In order to guarantee always positive values of the uncertain Young's modulus, the deviation amplitude of α_i^I must satisfy the condition $\Delta\alpha_i < 1$. Spatial variability of the uncertain elastic modulus is handled under the limit assumption that the fluctuations α_i^I vary independently. In this respect, it is worth emphasizing that an *EUI* is associated to each uncertain Young's modulus and therefore to each FE. This allows one to link the physical properties to the FEs and limit the overestimation due to the *dependency phenomenon* which typically affects both the assembly and solution phases of IFEMs based on the *CIA*. In order to obtain a more realistic description as well as a reduction of the computational effort, a different mesh can be adopted to describe the spatial variability of Young's modulus, i.e. the volume V can be subdivided into $N_r < N_e$ subdomains characterized by interval elastic moduli (see Eq. (4)) exhibiting independent variations caused for instance by different degradation, exposure or heterogeneity of the material. Under this assumption, the present formulation associates an *EUI* to each subdomain, as outlined in detail in Section 6.

Taking into account Eqs. (4) and (5), the elastic matrix of the i-th FE can be expressed as:

$$\mathbf{E}^{(i)}(\alpha_i^I) = \left(1+\Delta\alpha_i \hat{e}_i^I\right)\mathbf{E}_0^{(i)} \tag{6}$$

where $\mathbf{E}_0^{(i)}$ is the elastic matrix of the FE with nominal Young's modulus $E_0^{(i)}$.

Uncertainty affecting the elastic modulus of the material propagates to the response of the solid which turns out to be described by interval quantities. Specifically, following the standard displacement-based FE formulation, the interval displacement field within the i-th FE can be approximated as follows:

$$\mathbf{u}^{(i)}(\mathbf{x};\boldsymbol{\alpha}^I) = \mathbf{N}^{(i)}(\mathbf{x})\mathbf{d}^{(i)}(\boldsymbol{\alpha}^I) \tag{7}$$

where $\boldsymbol{\alpha}^I = [\underline{\boldsymbol{\alpha}}, \overline{\boldsymbol{\alpha}}] \in \mathbb{IR}^{N_e}$ is the interval vector collecting the dimensionless fluctuations α_i^I, ($i = 1, 2, \ldots, N^{(e)}$), of Young's moduli of the N_e FEs; $\mathbf{N}^{(i)}(\mathbf{x})$ denotes the shape-function matrix; $\mathbf{d}^{(i)}(\boldsymbol{\alpha}^I)$ is the nodal displacement vector of the i-th FE which depends on the interval variables α_i^I.

Strain-displacement equations yield the following expression of the interval strain field within the i-th FE:

$$\boldsymbol{\varepsilon}^{(i)}(\mathbf{x};\boldsymbol{\alpha}^I) = \mathbf{B}^{(i)}(\mathbf{x})\mathbf{d}^{(i)}(\boldsymbol{\alpha}^I) \tag{8}$$

where $\mathbf{B}^{(i)}(\mathbf{x})$ is the strain-displacement matrix. Finally, upon replacing Eqs. (6) and (8) into the linear-elastic constitutive equations, the interval stress field can be expressed as follows:

$$\boldsymbol{\sigma}^{(i)}(\mathbf{x};\boldsymbol{\alpha}^I) = \mathbf{E}^{(i)}(\alpha_i^I)\boldsymbol{\varepsilon}^{(i)}(\mathbf{x};\boldsymbol{\alpha}^I) = \left(1 + \Delta\alpha_i \hat{e}_i^I\right)\mathbf{E}_0^{(i)}\mathbf{B}^{(i)}(\mathbf{x})\mathbf{d}^{(i)}(\boldsymbol{\alpha}^I). \tag{9}$$

In analogy to the standard displacement-based FEM, Eqs. (7)-(9) express the interval displacement, strain and stress fields within the i-th FE as interpolation of the nodal displacements $\mathbf{d}^{(i)}(\boldsymbol{\alpha}^I)$. Notice that the interval stresses, collected into the vector $\boldsymbol{\sigma}^{(i)}(\mathbf{x};\boldsymbol{\alpha}^I)$, depend on the uncertain parameters both through the nodal displacements $\mathbf{d}^{(i)}(\boldsymbol{\alpha}^I)$ and the elastic matrix

$\mathbf{E}^{(i)}(\alpha_i^I)$. This circumstance makes the interval stress field more sensitive to the *dependency phenomenon* than the displacement field.

The stiffness matrix of the i-th FE is an interval matrix formally analogous to the one pertaining to the deterministic FE, i.e.:

$$\mathbf{k}^{(i)}(\alpha_i^I) = \int_{V^{(i)}} \mathbf{B}^{(i)\mathrm{T}}(\mathbf{x})\mathbf{E}^{(i)}(\alpha_i^I)\mathbf{B}^{(i)}(\mathbf{x})\mathrm{d}V^{(i)}. \tag{10}$$

Upon replacing the definition (6) of the interval elastic matrix, the previous equation can be recast as:

$$\mathbf{k}^{(i)}(\alpha_i^I) = \left(1 + \Delta\alpha_i \hat{e}_i^I\right)\mathbf{k}_0^{(i)} \tag{11}$$

where the matrix $\mathbf{k}^{(i)}(\alpha_i^I)$, depending only on the i-th interval variable, α_i^I, and, therefore on the i -th *EUI*, is conveniently expressed as the result of a fluctuation around the nominal stiffness matrix $\mathbf{k}_0^{(i)} = \mathbf{k}^{(i)}(\alpha_i)\big|_{\boldsymbol{\alpha}=\mathbf{0}}$, given by:

$$\mathbf{k}_0^{(i)} = \int_{V^{(i)}} \mathbf{B}^{(i)\mathrm{T}}(\mathbf{x})\mathbf{E}_0^{(i)}\mathbf{B}^{(i)}(\mathbf{x})\mathrm{d}V^{(i)} \tag{12}$$

$\mathbf{E}_0^{(i)}$ being the nominal elastic matrix.

Under the assumed hypothesis of deterministic applied loads, the element force vector is not affected by uncertainties, i.e.:

$$\mathbf{f}^{(i)} = \int_{V^{(i)}} \mathbf{N}^{(i)\mathrm{T}}(\mathbf{x})\mathbf{b}(\mathbf{x})\mathrm{d}V^{(i)} + \int_{S_t^{(i)}} \mathbf{N}^{(i)\mathrm{T}}(\mathbf{x})\mathbf{t}(\mathbf{x})\mathrm{d}S^{(i)}. \tag{13}$$

One of the main features of the proposed IFEM is that standard assembly procedure can be carried out. Indeed, by applying the *IIA via EUI*, an *EUI* is associated to the stiffness matrix of each FE (see Eq.(11)). During the assembly phase, this allows one to keep track of the dependencies between interval parameters representing FE physical properties and thus counteract one of the main sources of overestimation affecting IFEMs. For the sake of simplicity, it is assumed that the interval element stiffness matrices and the force vectors are referred to the global coordinate system, so that no coordinate transformation is needed. Then, as in the standard FEM, the nodal displacement vector of the i-th FE, $\mathbf{d}^{(i)}(\boldsymbol{\alpha}^I)$, can be related to the global nodal displacements collected into the interval vector $\mathbf{U}(\boldsymbol{\alpha}^I)$ as:

$$\mathbf{d}^{(i)}(\boldsymbol{\alpha}^I) = \mathbf{L}^{(i)}\mathbf{U}(\boldsymbol{\alpha}^I) \tag{14}$$

where $\mathbf{L}^{(i)}$ is a Boolean matrix defined so as to take into account the boundary conditions. Then, the assembly procedure yields the following set of linear interval equations governing the equilibrium of the FE model:

$$\mathbf{K}(\boldsymbol{\alpha}^I)\mathbf{U}(\boldsymbol{\alpha}^I) = \mathbf{F} \tag{15}$$

where

$$\mathbf{K}(\boldsymbol{\alpha}^I) \equiv \mathbf{K}^I = \sum_{i=1}^{N_e} \mathbf{L}^{(i)\mathrm{T}}\mathbf{k}^{(i)}(\alpha_i^I)\mathbf{L}^{(i)} \tag{16}$$

and

$$\mathbf{F} = \sum_{i=1}^{N_e} \mathbf{L}^{(i)\mathrm{T}}\mathbf{f}^{(i)} \tag{17}$$

are the interval global stiffness matrix and the nodal force vector, respectively.

Taking into account Eq.(11), the interval global stiffness matrix can be rewritten as sum of the nominal value plus an interval deviation, i.e.:

$$\mathbf{K}^I = \mathbf{K}_0 + \sum_{i=1}^{N_e} \mathbf{L}^{(i)\mathrm{T}}\mathbf{k}_0^{(i)}\mathbf{L}^{(i)}\Delta\alpha_i\hat{e}_i^I \tag{18}$$

where $\mathbf{K}_0 = \mathbf{K}(\boldsymbol{\alpha})\big|_{\boldsymbol{\alpha}=\mathbf{0}}$ and $\mathbf{k}_0^{(i)} = \mathbf{k}^{(i)}(\alpha_i)\big|_{\boldsymbol{\alpha}=\mathbf{0}}$ are the global and element nominal stiffness matrices, respectively. Notice that the interval deviation is given by the superposition of the contributions of the N_e uncertain parameters which are identified by the associated *EUI*s.

As already mentioned, the novel IFEM is formulated under the assumption that all input data except Young's modulus of the material are deterministic. In this regard, it is worth remarking that an expression of the interval global stiffness matrix analogous to that in Eq. (18) can be reasonably adopted also when geometrical uncertainties are considered. Indeed, if the element stiffness matrix is not proportional to the uncertain parameter (e.g. length of a truss or beam element, thickness of a bending plate element), the interval global stiffness matrix can be approximated according to Eq. (18) by applying a variable transformation and retaining just linear dependency on the uncertain parameters [23].

3.2 Approximate explicit solution by Interval Rational Series Expansion

The solution set of the interval global equilibrium equations (15), Σ, contains all possible solutions obtained as the uncertain parameters range over their intervals, i.e.:

$$\Sigma = \left\{ \mathbf{U} \in \mathbb{R}^n \,\middle|\, \mathbf{K}(\boldsymbol{\alpha})\mathbf{U}(\boldsymbol{\alpha}) = \mathbf{F},\ \boldsymbol{\alpha} \in \boldsymbol{\alpha}^I \right\} \tag{19}$$

where n is the order of the global displacement vector $\mathbf{U}(\boldsymbol{\alpha})$. The set Σ usually is not an interval vector and does not need to be convex [17]. The interval stiffness matrix $\mathbf{K}^I$ is regular, that is each matrix $\mathbf{K} \in \mathbf{K}^I$ is non-singular [36]. The regularity of the matrix $\mathbf{K}^I$ guarantees that the solution set is bounded. However, the exact evaluation of the solution set is very difficult since, typically, it is described by a complicated region in the output space. To circumvent this difficulty, in the framework of interval analysis, it is common practice to seek the interval displacement vector $\mathbf{U}^I$, containing the solution set Σ, which has the narrowest interval components. Thus, the aim is the evaluation of the LB and UB of the interval displacement vector $\mathbf{U}^I$, say $\underline{\mathbf{U}}(\boldsymbol{\alpha})$ and $\overline{\mathbf{U}}(\boldsymbol{\alpha})$. In this context, the knowledge of the explicit inverse of the interval stiffness matrix $\mathbf{K}^I$ plays a crucial role. Recently, the so-called *Interval Rational Series Expansion* (*IRSE*) [32-35] has been derived as a modified explicit form of the Neumann series for evaluating the approximate inverse of an interval matrix with small rank-r modifications. The first step to apply the *IRSE* is the decomposition of the interval stiffness matrix as sum of the nominal value plus an interval deviation given by a superposition of rank-one matrices. For this purpose, several strategies can be applied (see, e.g. [32-35]). In the present study, the spectral decomposition of the nominal element stiffness matrix is exploited, which yields:

$$\mathbf{K}^I = \mathbf{K}_0 + \sum_{i=1}^{N_e} \sum_{\ell=1}^{p_i} \lambda_i^{(\ell)} \mathbf{v}_i^{(\ell)} \mathbf{v}_i^{(\ell)\mathrm{T}} \Delta\alpha_i \, \hat{e}_i^I \tag{20}$$

where

$$\mathbf{v}_i^{(\ell)} = \mathbf{L}^{(i)\mathrm{T}} \boldsymbol{\phi}_i^{(\ell)}. \tag{21}$$

In the previous equations, $\lambda_i^{(\ell)}$ and $\boldsymbol{\phi}_i^{(\ell)}$ denote the ℓ-th eigenvalue and the associated eigenvector of the nominal stiffness matrix $\mathbf{k}_0^{(i)}$ of the i-th FE, solutions of the following eigenproblem:

$$\mathbf{k}_0^{(i)} \boldsymbol{\phi}_i^{(\ell)} = \lambda_i^{(\ell)} \boldsymbol{\phi}_i^{(\ell)} \qquad (i = 1, \ldots, N_e;\ \ell = 1, \ldots, p_i) \tag{22}$$

such that

$$\mathbf{k}_0^{(i)} = \sum_{\ell=1}^{p_i} \lambda_i^{(\ell)} \boldsymbol{\phi}_i^{(\ell)} \boldsymbol{\phi}_i^{(\ell)\mathrm{T}}. \tag{23}$$

Notice that only $p_i < n$ eigenvalues are different from zero, as many as are the deformation modes of the i-th FE. For instance, for a bar type FE only one eigenvalue is different from zero since the element is characterized by one deformation mode; a beam type FE has two deformation modes so that the solution of the eigenproblem (22) gives two non-zero eigenvalues. Thus, according to Eq. (20), the spectral decomposition allows one to express the interval deviation of the global stiffness matrix $\mathbf{K}^I$ with respect to the nominal value $\mathbf{K}_0$ as superposition of $N_e \times p_i$ matrices $\lambda_i^{(\ell)} \mathbf{v}_i^{(\ell)} \mathbf{v}_i^{(\ell)\mathrm{T}} \Delta\alpha_i \, \hat{e}_i^I$ of rank one, where p_i depends on the type of FE employed in the mesh.

By applying the *IRSE*, the following approximate explicit expression of the inverse of the interval stiffness matrix, $\mathbf{K}^I$, is obtained:

$$\left(\mathbf{K}^I\right)^{-1}=\left[\mathbf{K}_0+\sum_{i=1}^{N_e}\sum_{\ell=1}^{p_i}\lambda_i^{(\ell)}\mathbf{v}_i^{(\ell)}\mathbf{v}_i^{(\ell)\mathrm{T}}\Delta\alpha_i\,\hat{e}_i^I\right]^{-1}\approx\mathbf{K}_0^{-1}-\sum_{i=1}^{N_e}\sum_{\ell=1}^{p_i}\frac{\Delta\alpha_i\hat{e}_i^I\lambda_i^{(\ell)}}{1+\lambda_i^{(\ell)}\Delta\alpha_i\hat{e}_i^I d_{i\ell}}\mathbf{D}_{i\ell}$$
$$+\sum_{i=1}^{N_e}\sum_{\substack{j=1\\j\neq i}}^{N_e}\sum_{\ell=1}^{p_i}\sum_{q=1}^{p_j}\frac{\Delta\alpha_i\Delta\alpha_j\lambda_i^{(\ell)}\lambda_j^{(q)}\hat{e}_i^I\hat{e}_j^I}{1+\lambda_j^{(q)}\Delta\alpha_j\hat{e}_j^I d_{jq}}d_{ij\ell q}\mathbf{D}_{ij\ell q}-\ldots \tag{24}$$

where

$$d_{i\ell}=\mathbf{v}_i^{(\ell)\mathrm{T}}\mathbf{K}_0^{-1}\mathbf{v}_i^{(\ell)};\quad \mathbf{D}_{i\ell}=\mathbf{K}_0^{-1}\mathbf{v}_i^{(\ell)}\mathbf{v}_i^{(\ell)\mathrm{T}}\mathbf{K}_0^{-1};$$
$$d_{ij\ell q}=\mathbf{v}_i^{(\ell)\mathrm{T}}\mathbf{K}_0^{-1}\mathbf{v}_j^{(q)};\quad \mathbf{D}_{ij\ell q}=\mathbf{K}_0^{-1}\mathbf{v}_i^{(\ell)}\mathbf{v}_j^{(q)\mathrm{T}}\mathbf{K}_0^{-1}. \tag{25a-d}$$

Equation (24) holds if and only if the conditions $\left|\lambda_i^{(\ell)}\Delta\alpha_i d_{i\ell}\right|<1$ are satisfied [34]. Such conditions do not imply additional limitations on the deviation amplitudes $\Delta\alpha_i<1$ of the uncertain elastic moduli. Notice that the *IRSE* (24) keeps track of the dependencies between interval Young's moduli by means of the *EUI*s which are associated to each uncertain parameter.

It is worth mentioning that Eq. (24) differs from the approximate explicit expressions of the inverse of the interval stiffness matrix derived in previous papers by applying the *IRSE* [32-35] just for the use of the spectral decomposition of the nominal stiffness matrix of the FEs (see Eq. (20)). Such decomposition allows one to enhance the computational efficiency of the *IRSE* for the following main reasons: *i*) the number of series terms depends on the number of non-zero eigenvalues $p_i<n$ regardless of the size of the structure, namely it does not depend on the number of degrees-of-freedom (DOFs); *ii*) when a uniform mesh is adopted, only one eigenproblem (see Eq. (22)) needs to be solved.

For small degrees of uncertainty, as those commonly occurring in engineering practice, say $\Delta\alpha_i<<1$, the *IRSE* in Eq.(24) can be reasonably truncated to first-order terms obtaining the following formula:

$$\left(\mathbf{K}^{I}\right)^{-1}=\left[\mathbf{K}_{0}+\sum_{i=1}^{N_e}\sum_{\ell=1}^{p_i}\lambda_i^{(\ell)}\mathbf{v}_i^{(\ell)}\mathbf{v}_i^{(\ell)\mathrm{T}}\Delta\alpha_i\,\hat{e}_i^I\right]^{-1}\approx\mathbf{K}_0^{-1}-\sum_{i=1}^{N_e}\sum_{\ell=1}^{p_i}\frac{\Delta\alpha_i\hat{e}_i^I\lambda_i^{(\ell)}}{1+\lambda_i^{(\ell)}\Delta\alpha_i\hat{e}_i^I d_{i\ell}}\mathbf{D}_{i\ell} \tag{26}$$

which will be referred to in the sequel as *IRSE*-1.

As will be outlined in details next, in view of the evaluation of the bounds of the interval response, the *IRSE*-1 can be conveniently rewritten as follows:

$$\left(\mathbf{K}^{I}\right)^{-1}=\mathbf{K}_0^{-1}+\sum_{i=1}^{N_e}\sum_{\ell=1}^{p_i}\left(a_{0,i\ell}-\Delta a_{i\ell}\hat{e}_i^I\right)\mathbf{D}_{i\ell} \tag{27}$$

where $a_{0,i\ell}$ and $\Delta a_{i\ell}$ are the midpoint and deviation amplitude of the generic term of the double summation in Eq. (26) rewritten in *affine form*, given by:

$$a_{0,i\ell}=\frac{\left(\lambda_i^{(\ell)}\Delta\alpha_i\right)^2 d_{i\ell}}{1-\left(\lambda_i^{(\ell)}\Delta\alpha_i d_{i\ell}\right)^2};\qquad \Delta a_{i\ell}=\frac{\lambda_i^{(\ell)}\Delta\alpha_i}{1-\left(\lambda_i^{(\ell)}\Delta\alpha_i d_{i\ell}\right)^2}. \tag{28a,b}$$

The argument $\Delta\alpha_i$ of the functions $a_{0,i\ell}$ and $\Delta a_{i\ell}$ is omitted for conciseness. It is worth remarking that the *EUI*s appearing in Eq. (27) are still associated to each uncertain parameter.

4. BOUNDS OF THE SOLUTION: APPROACH BASED ON THE AFFINE FORM

4.1 Bounds of interval displacements

The evaluation of the approximate inverse of the interval stiffness matrix by the *IRSE* allows one to derive the interval global displacement vector $\mathbf{U}^I$ in approximate explicit form. In particular, if the deviation amplitudes of the uncertain parameters satisfy the conditions $\Delta\alpha_i << 1$, the *IRSE*-1 (27) leads to express $\mathbf{U}^I$ as sum of the midpoint value plus an interval deviation. i.e.:

$$\mathbf{U}^I\equiv\mathbf{U}(\boldsymbol{\alpha}^I)=\left(\mathbf{K}^I\right)^{-1}\mathbf{F}=\mathrm{mid}\left\{\mathbf{U}(\boldsymbol{\alpha}^I)\right\}+\mathrm{dev}\left\{\mathbf{U}(\boldsymbol{\alpha}^I)\right\} \tag{29}$$

where

$$\mathrm{mid}\left\{\mathbf{U}^{I}\right\}=\mathbf{K}_0^{-1}\mathbf{F}+\sum_{i=1}^{N_e}\sum_{\ell=1}^{p_i}a_{0,i\ell}\,\mathbf{D}_{i\ell}\mathbf{F};$$

$$\mathrm{dev}\left\{\mathbf{U}^{I}\right\}=-\sum_{i=1}^{N_e}\sum_{\ell=1}^{p_i}\;\Delta a_{i\ell}\,\hat{e}_i^{I}\,\mathbf{D}_{i\ell}\mathbf{F}=\sum_{i=1}^{N_e}\mathbf{R}_i\hat{e}_i^{I} \qquad (30a,b)$$

with

$$\mathbf{R}_i=-\sum_{\ell=1}^{p_i}\;\Delta a_{i\ell}\mathbf{D}_{i\ell}\mathbf{F}. \qquad (31)$$

In Eq. (29), $\mathrm{dev}\{\bullet\}$ is an operator which yields the interval deviation of the quantity between curly brackets. By inspection of Eq. (30b), it is observed that the *IRSE*-1 enables to express the interval deviation of the displacement vector as superposition of the contributions of the N_e uncertain parameters each one identified by a different *EUI*.

Based on Eq. (29) and applying the *IIA via EUI*, the following approximate explicit expressions of the LB and UB of the interval displacement vector $\mathbf{U}^I$ are obtained:

$$\underline{\mathbf{U}}(\boldsymbol{\alpha})=\mathrm{mid}\left\{\mathbf{U}^{I}\right\}-\Delta\mathbf{U}(\boldsymbol{\alpha});$$

$$\overline{\mathbf{U}}(\boldsymbol{\alpha})=\mathrm{mid}\left\{\mathbf{U}^{I}\right\}+\Delta\mathbf{U}(\boldsymbol{\alpha}) \qquad (32a,b)$$

where

$$\Delta\mathbf{U}(\boldsymbol{\alpha})=\sum_{i=1}^{N_e}\left|\mathbf{R}_i\right|=\sum_{i=1}^{N_e}\left|\sum_{\ell=1}^{p_i}\Delta a_{i\ell}\mathbf{D}_{i\ell}\mathbf{F}\right| \qquad (33)$$

is the deviation amplitude of $\mathbf{U}^I$ and the symbol $|\bullet|$ denotes absolute value component wise.

Once the bounds of the interval nodal displacements are known, the LB and UB of the displacement field within the generic FE can be determined based on Eqs. (7) and (14), as in the standard FEM.

4.2 Bounds of interval stresses

By applying the *IRSE*, the interval stress field (9) within the i-th FE, $\boldsymbol{\sigma}^{(i)}(\mathbf{x};\boldsymbol{\alpha}^I)$, can be expressed in approximate explicit form as well. Specifically, taking into account Eq. (14) and evaluating $\mathbf{U}^I = \left(\mathbf{K}^I\right)^{-1}\mathbf{F}$ by means of the *IRSE*-1 (see Eq.(27)), Eq. (9) yields:

$$\begin{aligned}\boldsymbol{\sigma}^{(i)}(\mathbf{x};\boldsymbol{\alpha}^I) &= \left(1+\Delta\alpha_i\hat{e}_i^I\right)\mathbf{E}_0^{(i)}\mathbf{B}^{(i)}(\mathbf{x})\mathbf{L}^{(i)}\left(\mathbf{K}^I\right)^{-1}\mathbf{F} \\ &= \left(1+\Delta\alpha_i\hat{e}_i^I\right)\mathbf{C}_0^{(i)}(\mathbf{x})\left[\mathbf{K}_0^{-1}+\sum_{j=1}^{N_e}\sum_{\ell=1}^{p_i}\left(a_{0,j\ell}-\Delta a_{j\ell}\hat{e}_j^I\right)\mathbf{D}_{j\ell}\right]\mathbf{F}\end{aligned} \tag{34}$$

where

$$\mathbf{C}_0^{(i)}(\mathbf{x}) = \mathbf{E}_0^{(i)}\mathbf{B}^{(i)}(\mathbf{x})\mathbf{L}^{(i)}. \tag{35}$$

Equation (34) holds under the assumption of small deviation amplitudes of the uncertain parameters, say $\Delta\alpha_i << 1$.

It is worth observing that the interval stress field $\boldsymbol{\sigma}^{(i)}(\mathbf{x};\boldsymbol{\alpha}^I)$ within the i-th FE is more affected by the *dependency phenomenon* than the interval displacement vector $\mathbf{U}^I$ due to the double occurrence of the *EUI*, $\hat{e}_i^I$, associated to the i-th uncertain parameter (see Eq. (34)). In order to limit the overestimation of the interval stress field range, Eq. (34) is rewritten in the following form:

$$\boldsymbol{\sigma}^{(i)}(\mathbf{x};\boldsymbol{\alpha}^I) = \left(1+\Delta\alpha_i\hat{e}_i^I\right)\mathbf{C}_0^{(i)}(\mathbf{x})\left[\mathbf{K}_0^{-1}\mathbf{F}+\sum_{j=1}^{N_e}\sum_{\ell=1}^{p_i}a_{0,j\ell}\mathbf{D}_{j\ell}\mathbf{F}+\mathbf{R}_i\hat{e}_i^I+\sum_{\substack{j=1\\j\neq i}}^{N_e}\mathbf{R}_j\hat{e}_j^I\right] \tag{36}$$

where the contribution of the i-th uncertain parameter is isolated from the remaining ones and $\mathbf{R}_i$ is given by Eq.(31). Based on Eq. (36) and applying the *IIA via EUI*, let us define the following pair of interval vectors:

$$\begin{aligned}\boldsymbol{\sigma}^{(i)-}(\mathbf{x};\alpha_i^I) &= \left(1+\Delta\alpha_i\hat{e}_i^I\right)\left\{\mathbf{C}_0^{(i)}(\mathbf{x})\left[\mathrm{mid}\left\{\mathbf{U}^I\right\}+\mathbf{R}_i\hat{e}_i^I\right]-\sum_{\substack{j=1\\j\neq i}}^{N_e}\left|\mathbf{C}_0^{(i)}(\mathbf{x})\mathbf{R}_j\right|\right\}; \\ \boldsymbol{\sigma}^{(i)+}(\mathbf{x};\alpha_i^I) &= \left(1+\Delta\alpha_i\hat{e}_i^I\right)\left\{\mathbf{C}_0^{(i)}(\mathbf{x})\left[\mathrm{mid}\left\{\mathbf{U}^I\right\}+\mathbf{R}_i\hat{e}_i^I\right]+\sum_{\substack{j=1\\j\neq i}}^{N_e}\left|\mathbf{C}_0^{(i)}(\mathbf{x})\mathbf{R}_j\right|\right\}\end{aligned} \tag{37a,b}$$

where the superscripts are related to the sign minus or plus before the summation within curly brackets and the definition (30a) of the midpoint value of the interval displacement vector $\mathbf{U}^I$ has been taken into account. It can be readily verified, that if Young's modulus of the i-th FE is deterministic, i.e. $\hat{e}_i^I = 0$, Eqs.(37a,b) yield the LB and UB of the interval stress vector $\boldsymbol{\sigma}^{(i)}(\mathbf{x};\boldsymbol{\alpha}^I)$, respectively. Then, taking into account that the interval vectors in Eqs. (37a,b) depend on a single interval parameter, say $\alpha_i^I = \Delta\alpha_i \hat{e}_i^I$, the LB and UB of the h-th interval stress component within the i-th FE, $\sigma_h^{(i)}(\mathbf{x};\boldsymbol{\alpha}^I)$, can be evaluated as follows:

$$\begin{aligned} \underline{\sigma}_h^{(i)}(\mathbf{x};\boldsymbol{\alpha}) &= \min_{\alpha_i \in \alpha_i^I = \Delta\alpha_i \hat{e}_i^I} \left\{ \sigma_h^{(i)-}\left(\mathbf{x};\alpha_i^I\right) \right\} = \min\left\{ \sigma_h^{(i)-}\left(\mathbf{x};-\Delta\alpha_i\right), \sigma_h^{(i)-}\left(\mathbf{x};\Delta\alpha_i\right) \right\}; \\ \overline{\sigma}_h^{(i)}(\mathbf{x};\boldsymbol{\alpha}) &= \max_{\alpha_i \in \alpha_i^I = \Delta\alpha_i \hat{e}_i^I} \left\{ \sigma_h^{(i)+}\left(\mathbf{x};\alpha_i^I\right) \right\} = \max\left\{ \sigma_h^{(i)+}\left(\mathbf{x};-\Delta\alpha_i\right), \sigma_h^{(i)+}\left(\mathbf{x};\Delta\alpha_i\right) \right\}. \end{aligned} \quad \text{(38a,b)}$$

Notice that, since the stress field is a monotonic function of the i-th uncertain parameter $\alpha_i^I = \Delta\alpha_i \hat{e}_i^I$, just two combinations corresponding to the endpoints of $\hat{e}_i^I$, i.e. $\underline{\alpha}_i = -\Delta\alpha_i$ and $\overline{\alpha}_i = \Delta\alpha_i$, need to be explored in order to evaluate the LB and UB of $\sigma_h^{(i)}(\mathbf{x};\boldsymbol{\alpha}^I)$.

The knowledge of the bounds of the interval nodal stresses enables to the determine the LB and UB of the stress field within each FE following standard post-processing rules, i.e. by applying Eqs. (9) and (14).

5. BOUNDS OF THE SOLUTION: SENSITIVITY BASED APPROACH

5.1 Bounds of interval displacements

The procedure for the evaluation of the bounds of the interval displacements and stresses outlined in the previous section relies on the use of the *IRSE*-1 rewritten in *affine form* (see Eq. (27)). As already mentioned, the *IRSE*-1 is accurate as long as small degrees of uncertainty are considered, i.e. $\Delta\alpha_i << 1$. If the interval parameters exhibit large deviation amplitudes, then higher-order terms of the *IRSE* need to be retained. Besides the increase of computational effort, a main drawback associated to the inclusion of higher-order terms is the additional overestimation of the interval solution range due to the *dependency phenomenon*. To cope with this problem, in the present study, the LB and UB of the interval response are evaluated by performing a preliminary sensitivity analysis which enables to predict the monotonic behaviour with respect to the uncertain parameters.

The *IRSE* (24) with an arbitrary number of series terms provides the interval displacement vector $\mathbf{U}^I$ as an approximate explicit function of the N_e uncertain parameters $\alpha_i^I = \Delta\alpha_i \, \hat{e}_i^I$, $(i = 1, 2, \ldots, N_e)$, i.e.:

$$\mathbf{U}^I = \left(\mathbf{K}^I\right)^{-1} \mathbf{F} \approx \left[\mathbf{K}_0^{-1} - \sum_{i=1}^{N_e} \sum_{\ell=1}^{p_i} \frac{\alpha_i^I \lambda_i^{(\ell)}}{1 + \lambda_i^{(\ell)} \alpha_i^I d_{i\ell}} \mathbf{D}_{i\ell} + \sum_{i=1}^{N_e} \sum_{\substack{j=1 \\ j \neq i}}^{N_e} \sum_{\ell=1}^{p_i} \sum_{q=1}^{p_j} \frac{\lambda_i^{(\ell)} \lambda_j^{(q)} \alpha_i^I \alpha_j^I}{1 + \lambda_j^{(q)} \alpha_j^I d_{jq}} d_{ij\ell q} \mathbf{D}_{ij\ell q} - \ldots \right] \mathbf{F} \tag{39}$$
$$\equiv \mathbf{U}\left(\alpha_1^I, \alpha_2^I, \ldots, \alpha_{N_e}^I\right).$$

By direct differentiation of the previous equation, the vector collecting sensitivities of the displacements to the i-th uncertain parameter can be derived in the following explicit form:

$$\mathbf{s}_{\mathbf{U},i} = \left. \frac{\partial \mathbf{U}(\boldsymbol{\alpha})}{\partial \alpha_i} \right|_{\boldsymbol{\alpha}=\mathbf{0}} = -\sum_{\ell=1}^{p_i} \lambda_i^{(\ell)} \mathbf{D}_{i\ell} \mathbf{F}, \quad (i = 1, 2, \ldots, N_e). \tag{40}$$

As known, the j-th component, $s_{U_j,i}$, of the sensitivity vector, $\mathbf{s}_{\mathbf{U},i}$, defined in Eq. (40) gives information about the change of the displacement $U_j(\boldsymbol{\alpha})$ due to a variation of the i-th structural parameter α_i with respect to the nominal value. Specifically, within a small range around $\boldsymbol{\alpha} = \mathbf{0}$, $U_j(\boldsymbol{\alpha})$ is an increasing or decreasing function of the parameter α_i depending on whether $s_{U_j,i} > 0$ or $s_{U_j,i} < 0$, respectively. Then, based on the knowledge of the sensitivities $s_{U_j,i}$ $(i = 1, 2, \ldots, N_e)$, the combinations of the extreme values of the uncertain parameters providing the LB and UB of the j-th displacement component U_j^I, denoted by $\alpha_{j,i}^{(\mathrm{LB})}$ and $\alpha_{j,i}^{(\mathrm{UB})}$, respectively, can be determined as follows:

$$\begin{aligned}&\text{if} \quad s_{U_j,i} > 0, \quad \text{then} \quad \alpha_{j,i}^{(\mathrm{UB})} = \bar{\alpha}_i, \quad \alpha_{j,i}^{(\mathrm{LB})} = \underline{\alpha}_i;\\ &\text{if} \quad s_{U_j,i} < 0, \quad \text{then} \quad \alpha_{j,i}^{(\mathrm{UB})} = \underline{\alpha}_i, \quad \alpha_{j,i}^{(\mathrm{LB})} = \bar{\alpha}_i, \quad (j = 1,2,\ldots,n; \;\; i = 1,2,\ldots,N_e).\end{aligned} \tag{41a,b}$$

The parameters $\alpha_{j,i}^{(\mathrm{LB})}$ and $\alpha_{j,i}^{(\mathrm{UB})}$ can be collected into the following vectors:

$$\begin{aligned}\boldsymbol{\alpha}_j^{(\mathrm{LB})} &= \left[\alpha_{j,1}^{(\mathrm{LB})} \quad \alpha_{j,2}^{(\mathrm{LB})} \quad \ldots \quad \alpha_{j,N_e}^{(\mathrm{LB})} \right]^{\mathrm{T}};\\ \boldsymbol{\alpha}_j^{(\mathrm{UB})} &= \left[\alpha_{j,1}^{(\mathrm{UB})} \quad \alpha_{j,2}^{(\mathrm{UB})} \quad \ldots \quad \alpha_{j,N_e}^{(\mathrm{UB})} \right]^{\mathrm{T}}, \quad (j = 1,2,\ldots,n).\end{aligned} \tag{42a,b}$$

Then, the LB and UB of the interval displacement component U_j^I can be evaluated in approximate explicit form by replacing the above defined combinations of the uncertain parameters into Eq. (39) where the desired number of series terms is retained, i.e.:

$$\underline{U}_j = U_j\left(\boldsymbol{\alpha}_j^{(\mathrm{LB})}\right); \quad \bar{U}_j = U_j\left(\boldsymbol{\alpha}_j^{(\mathrm{UB})}\right), \quad (j = 1,2,\ldots,n). \tag{43a,b}$$

It is worth mentioning that, once the equilibrium equations (15) are assembled taking advantage of the *IIA via EUI*, the main difference between the proposed approach and other methods based on sensitivity analysis (see e.g. [15,37]) lies in the use of the *IRSE* which yields the bounds of the solution in approximate explicit form and provides substantial computational advantages. Indeed, the proposed approach evaluates the LB and UB of the *j*-th displacement component according to Eqs. (43a,b) by replacing the parameters $\alpha_{j,i}^{(\mathrm{LB})}$ and $\alpha_{j,i}^{(\mathrm{UB})}$ into the explicit expression of the solution (39) given by the *IRSE* instead of performing the numerical inversion of the stiffness matrix for $\boldsymbol{\alpha} = \boldsymbol{\alpha}_j^{(\mathrm{LB})}$ and $\boldsymbol{\alpha} = \boldsymbol{\alpha}_j^{(\mathrm{UB})}$. Furthermore, sign sensitivities can be analyzed taking advantage of the explicit expressions of response sensitivities given by Eq. (40). Though this procedure is more computationally demanding than the one based on the *affine form* (see Section 4), it enables to retain higher-order terms of the *IRSE* which are needed in the presence of larger deviation amplitudes of the uncertain parameters. In this regard, it has to be observed that the computational efficiency of the proposed IFEM can be greatly enhanced by performing a preliminary sensitivity analysis [33] which allows one to identify the least influential uncertain parameters and then neglect the associated contributions in the *IRSE*.

5.2 Bounds of interval stresses

The sensitivity based approach can also be applied to evaluate the bounds of the interval stresses when higher-order terms of the *IRSE* (24) are retained. In this case, the interval stress vector (9) within the i-th FE is approximated by the following explicit function of the uncertain parameters $\alpha_i^I = \Delta\alpha_i \hat{e}_i^I$, $(i = 1, 2, \ldots, N_e)$:

$$\begin{aligned}\boldsymbol{\sigma}^{(i)}(\mathbf{x};\boldsymbol{\alpha}^I) \approx \left(1+\Delta\alpha_i\hat{e}_i^I\right)\mathbf{C}_0^{(i)}(\mathbf{x})\Bigg[\mathbf{K}_0^{-1} - \sum_{i=1}^{N_e}\sum_{\ell=1}^{p_i}\frac{\alpha_i^I\lambda_i^{(\ell)}}{1+\lambda_i^{(\ell)}\alpha_i^I d_{i\ell}}\mathbf{D}_{i\ell} \\ + \sum_{i=1}^{N_e}\sum_{\substack{j=1\\ j\neq i}}^{N_e}\sum_{\ell=1}^{p_i}\sum_{q=1}^{p_j}\frac{\lambda_i^{(\ell)}\lambda_j^{(q)}\alpha_i^I\alpha_j^I}{1+\lambda_j^{(q)}\alpha_j^I d_{jq}} d_{ij\ell q}\mathbf{D}_{ij\ell q} - \ldots\Bigg]\mathbf{F} \equiv \boldsymbol{\sigma}^{(i)}(\mathbf{x};\alpha_1^I,\alpha_2^I,\ldots,\alpha_{N_e}^I)\end{aligned} \tag{44}$$

where $\mathbf{C}_0^{(i)}(\mathbf{x})$ is the matrix defined in Eq.(35).

By direct differentiation of the previous equation, the vector collecting sensitivities of the stress components to the j-th uncertain parameter can be derived in the following explicit form:

$$\begin{aligned}\mathbf{s}_{\boldsymbol{\sigma}^{(i)},j}(\mathbf{x}) &= \left.\frac{\partial\boldsymbol{\sigma}^{(i)}(\mathbf{x};\boldsymbol{\alpha}^I)}{\partial\alpha_j}\right|_{\boldsymbol{\alpha}=\mathbf{0}} = \mathbf{C}_0^{(i)}(\mathbf{x})\left[\mathbf{K}_0^{-1} - \sum_{\ell=1}^{p_i}\lambda_i^{(\ell)}\mathbf{D}_{i\ell}\right]\mathbf{F}, \quad (i = j = 1, 2, \ldots, N_e); \\ \mathbf{s}_{\boldsymbol{\sigma}^{(i)},j}(\mathbf{x}) &= \left.\frac{\partial\boldsymbol{\sigma}^{(i)}(\mathbf{x};\boldsymbol{\alpha}^I)}{\partial\alpha_j}\right|_{\boldsymbol{\alpha}=\mathbf{0}} = -\mathbf{C}_0^{(i)}(\mathbf{x})\sum_{\ell=1}^{p_i}\lambda_j^{(\ell)}\mathbf{D}_{j\ell}\mathbf{F}, \qquad (i \neq j = 1, 2, \ldots, N_e).\end{aligned} \tag{45a,b}$$

By analysing the sign of sensitivities defined in Eqs. (45a,b), the change of the stress components due to a variation of the j-th structural parameter α_j with respect to the nominal value can be predicted. Specifically, within a small range around $\boldsymbol{\alpha} = \mathbf{0}$, the h-th stress component at the position $\mathbf{x}$ within the i-th FE, $\sigma_h^{(i)}(\mathbf{x};\boldsymbol{\alpha})$, turns out to be an increasing or decreasing function of the parameter α_j depending on whether $s_{\sigma_h^{(i)},j}(\mathbf{x}) > 0$ or $s_{\sigma_h^{(i)},j}(\mathbf{x}) < 0$, respectively. Based on the knowledge of the sensitivities $s_{\sigma_h^{(i)},j}(\mathbf{x})$, the combinations of the extreme values of the uncertain parameters providing the LB and UB of the h-th stress component $\sigma_h^{(i)}(\mathbf{x};\boldsymbol{\alpha}^I)$ within the i-th FE, denoted by $\alpha_{i,h,j}^{(\mathrm{LB})}$ and $\alpha_{i,h,j}^{(\mathrm{UB})}$, respectively, can be determined as follows:

$$\begin{aligned}&\text{if}\quad s_{\sigma_h^{(i)},j}(\mathbf{x})>0,\quad \text{then}\quad \alpha_{i,h,j}^{(\mathrm{UB})}=\overline{\alpha}_j,\quad \alpha_{i,h,j}^{(\mathrm{LB})}=\underline{\alpha}_j;\\ &\text{if}\quad s_{\sigma_h^{(i)},j}(\mathbf{x})<0,\quad \text{then}\quad \alpha_{i,h,j}^{(\mathrm{UB})}=\underline{\alpha}_j,\quad \alpha_{i,h,j}^{(\mathrm{LB})}=\overline{\alpha}_j,\quad (h=1,2,\ldots,n_s;\ j=1,2,\ldots,N_e)\end{aligned} \tag{46a,b}$$

where n_s denotes the number of stress components. The parameters $\alpha_{i,h,j}^{(\mathrm{LB})}$ and $\alpha_{i,h,j}^{(\mathrm{UB})}$ defined in Eqs. (46a,b) can be collected into the following vectors:

$$\begin{aligned}&\boldsymbol{\alpha}_{i,h}^{(\mathrm{LB})}=\left[\alpha_{i,h,1}^{(\mathrm{LB})}\quad \alpha_{i,h,2}^{(\mathrm{LB})}\quad \ldots\quad \alpha_{i,h,N_e}^{(\mathrm{LB})}\right]^{\mathrm{T}};\\ &\boldsymbol{\alpha}_{i,h}^{(\mathrm{UB})}=\left[\alpha_{i,h,1}^{(\mathrm{UB})}\quad \alpha_{i,h,2}^{(\mathrm{UB})}\quad \ldots\quad \alpha_{i,h,N_e}^{(\mathrm{UB})}\right]^{\mathrm{T}},\quad (h=1,2,\ldots,n_s;\ i=1,2,\ldots,N_e).\end{aligned} \tag{47a,b}$$

Then, the LB and UB of the interval stress component $\sigma_h^{(i)}\left(\mathbf{x};\boldsymbol{\alpha}^I\right)$ can be derived in approximate explicit form by replacing the above defined combinations of the uncertain parameters into Eq. (44), where the desired number of series terms is retained, i.e.:

$$\begin{aligned}&\underline{\sigma}_h^{(i)}(\mathbf{x};\boldsymbol{\alpha})=\sigma_h^{(i)}\left(\mathbf{x};\boldsymbol{\alpha}_{i,h}^{(\mathrm{LB})}\right);\\ &\overline{\sigma}_h^{(i)}(\mathbf{x};\boldsymbol{\alpha})=\sigma_h^{(i)}\left(\mathbf{x};\boldsymbol{\alpha}_{i,h}^{(\mathrm{UB})}\right),\quad (h=1,2,\ldots,n_s;\ \ i=1,2,\ldots,N_e).\end{aligned} \tag{48a,b}$$

Notice that the sensitivity based procedure may be computationally onerous since the vectors defined in Eqs. (47a,b) need to be determined for each stress component and each FE. However, the method enables to retain higher-order terms in the *IRSE* and proves to be very useful when the bounds of the stress at a selected point are of interest.

6. INDEPENDENT UNCERTAINTIES OVER SELECTED REGIONS

Allowing independent variations of Young's moduli of the FEs may be disadvantageous for the following main reasons: overestimation of the actual uncertainty, mesh-dependency of the solution and increase of the computational effort. The proposed IFEM enables to overcome these drawbacks by adopting two different meshes to describe the spatial variability of the uncertain property and the structural behaviour. To this aim, let us subdivide the body into $N_r < N_e$ regions or subdomains exhibiting independent variations of the interval Young's modulus, $E^{(j)}(\alpha_j^I) = E_0(1+\Delta\alpha_j \hat{e}_j^I)$, $j = 1, 2, \ldots, N_r$, with the j-th region including $N_e^{(j)}$ FEs. The collection of such regions is herein referred to as "uncertainty mesh". A finer uncertainty mesh implies independent variations of the elastic modulus at more closely spaced locations and therefore a higher degree of variability over the body domain. Obviously, the formulation of the IFEM developed in the previous sections assuming $N_r = N_e$ (and $N_e^{(j)} = 1$) still applies. For the sake of clarity, in the sequel just the basic formulas are specialized to the case of uncertainty mesh consisting of $N_r < N_e$ regions.

By applying the decomposition described in Section 3.2, the interval global stiffness matrix can be still expressed as sum of the nominal value plus a superposition of rank-one matrices, i.e.:

$$\mathbf{K}^I = \mathbf{K}_0 + \sum_{j=1}^{N_r} \Delta\alpha_j \hat{e}_j^I \sum_{i=1}^{N_e^{(j)}} \sum_{\ell=1}^{p_i} \lambda_i^{(\ell)} \mathbf{v}_i^{(\ell)} \mathbf{v}_i^{(\ell)\mathrm{T}} \tag{49}$$

where an *EUI* is linked to each subdomain with uncertain Young's modulus. Specifically, the j-th *EUI*, $\hat{e}_j^I$, is associated to all the $N_e^{(j)}$ FEs belonging to the j-th region with interval elastic modulus $E^{(j)}(\alpha_j^I) = E_0(1+\Delta\alpha_j \hat{e}_j^I)$.

Taking into account Eq. (49) and performing simple manipulations of the *IRSE*-1 (26), the following *affine form* expression of the approximate inverse of the interval global stiffness matrix is obtained:

$$\left(\mathbf{K}^I\right)^{-1} = \mathbf{K}_0^{-1} + \sum_{j=1}^{N_r} \sum_{i=1}^{N_e^{(j)}} \sum_{\ell=1}^{p_i} \left(a_{0,i\ell}^{(j)} - \Delta a_{i\ell}^{(j)} \hat{e}_j^I\right) \mathbf{D}_{i\ell} \tag{50}$$

where

$$a_{0,i\ell}^{(j)} = \frac{\left(\lambda_i^{(\ell)}\Delta\alpha_j\right)^2 d_{i\ell}}{1-\left(\lambda_i^{(\ell)}\Delta\alpha_j d_{i\ell}\right)^2}; \qquad \Delta a_{i\ell}^{(j)} = \frac{\lambda_i^{(\ell)}\Delta\alpha_j}{1-\left(\lambda_i^{(\ell)}\Delta\alpha_j d_{i\ell}\right)^2}. \tag{51a,b}$$

Notice that the *EUI*s in Eq. (50) are associated to the N_r regions with uncertain Young's modulus, thus allowing one to keep track of dependencies between interval variables and reduce the overestimation. Furthermore, FE refinement does not alter the description of the spatial variability of uncertainty since the number $N_r < N_e$ of the uncertain parameters over the entire structure is kept fixed.

Equation (50) enables to express the interval displacement vector as sum of the midpoint value plus an interval deviation (see Eq.(29)) and then evaluate the LB and UB vectors in approximate explicit form by means of Eqs. (32a,b) where:

$$\begin{aligned} \text{mid}\left\{\mathbf{U}^I\right\} &= \mathbf{K}_0^{-1}\mathbf{F} + \sum_{j=1}^{N_r}\sum_{i=1}^{N_e^{(j)}}\sum_{\ell=1}^{p_i} a_{0,i\ell}^{(j)}\mathbf{D}_{i\ell}\mathbf{F}\,; \\ \Delta\mathbf{U}(\boldsymbol{\alpha}) &= \sum_{i=1}^{N_r}\left|\sum_{i=1}^{N_e^{(j)}}\sum_{\ell=1}^{p_i}\ \Delta a_{i\ell}^{(j)}\mathbf{D}_{i\ell}\mathbf{F}\right|. \end{aligned} \tag{52a,b}$$

7. NUMERICAL APPLICATIONS

For validation purpose, three numerical examples concerning 2D and 3D FE modelled structures with uncertain Young's modulus, are presented.

The accuracy of the proposed IFEM is herein assessed by performing appropriate comparisons with the exact bounds of the response evaluated by applying a combinatorial procedure, known as *vertex method*, first introduced by Dong and Shah [38]. This method computes the LB and UB of the response quantity of interest as the minimum and maximum among the deterministic solutions pertaining to all possible combinations of the endpoints of the interval parameters, say 2^{N_e}. Obviously, this procedure is time-consuming and, unlike the proposed method, it becomes unfeasible when a large number of uncertain parameters is considered.

In cases involving a large number of uncertainties, the proposed method is validated by comparison with the solution computed by applying a sensitivity method (*SM*), conceptually analogous to the approach described in Section 5, which requires the following steps:

i) evaluate the exact sensitivities of nodal displacements as:

$$\left.\frac{\partial \mathbf{K}(\boldsymbol{\alpha}^I)}{\partial \alpha_i}\right|_{\boldsymbol{\alpha}=\mathbf{0}} \mathbf{U}_0 + \mathbf{K}_0 \left.\frac{\partial \mathbf{U}(\boldsymbol{\alpha}^I)}{\partial \alpha_i}\right|_{\boldsymbol{\alpha}=\mathbf{0}} = \mathbf{0} \Rightarrow \mathbf{s}_{\mathbf{U},i} = \left.\frac{\partial \mathbf{U}(\boldsymbol{\alpha}^I)}{\partial \alpha_i}\right|_{\boldsymbol{\alpha}=\mathbf{0}} = -\mathbf{K}_0^{-1}\mathbf{K}_i\mathbf{U}_0, \quad (i=1,2,\ldots,N_e); \qquad (53)$$

ii) based on Eqs. (41a,b), determine the vectors, $\boldsymbol{\alpha}_j^{(\mathrm{LB})}$ and $\boldsymbol{\alpha}_j^{(\mathrm{UB})}$, collecting the combinations of the endpoints of the uncertain parameters which give the LB and UB of j-th displacement component;

iii) evaluate the bounds $\underline{U}_j$ and $\overline{U}_j$ as the j-th component of the following vectors:

$$\mathbf{U}\left(\boldsymbol{\alpha}_j^{(\mathrm{LB})}\right) = \mathbf{K}^{-1}\left(\boldsymbol{\alpha}_j^{(\mathrm{LB})}\right)\mathbf{F}; \quad \mathbf{U}\left(\boldsymbol{\alpha}_j^{(\mathrm{UB})}\right) = \mathbf{K}^{-1}\left(\boldsymbol{\alpha}_j^{(\mathrm{UB})}\right)\mathbf{F}. \qquad (54a,b)$$

A similar procedure can be adopted to compute the LB and UB of the stress components.

Though more onerous from a computational point of view, the described method is more accurate than the sensitivity-based approach proposed in Section 5 which is affected by the approximation of the inverse of the interval stiffness matrix by means of the *IRSE*.

7.1 Square plate with uncertain Young's modulus: load condition 1

First, the proposed IFEM is applied to a plane stress problem, i.e. a square plate under uniform traction (load condition 1 (LC1)) with uncertain Young's modulus of the material (Figure 1). The following data are assumed: width and thickness of the plate $L = 0.1\,\mathrm{m}$ and $t = 0.001\,\mathrm{m}$, respectively; nominal Young's modulus $E_0 = 210\,\mathrm{GPa}$ and Poisson ratio $\nu = 0.3$; traction $p = 10\,\mathrm{MPa}$.

7.1.1 Independent uncertain Young's modulus for each FE

First, a uniform mesh consisting of $N_e = 16$ (Figure 1a) four-node 2D FEs is adopted. Young's moduli of the FEs are modelled as interval variables $E^{(i)}(\alpha_i^I) = E_0(1 + \Delta\alpha_i \hat{e}_i^I)$, where the same deviation amplitude $\Delta\alpha_i = \Delta\alpha$, $i = 1, 2, \ldots, N_e$, of the dimensionless fluctuations around the nominal value is assumed. Depending on the physical problem, the deviation amplitude may be different for the various uncertain parameters and its rigorous estimation should rely on available experimental data. In order to assess the capability of the IFEM based on the *IIA via EUI* to handle large fluctuations of the uncertain parameters, the deviation amplitude is set to $\Delta\alpha = 0.1$ and $\Delta\alpha = 0.2$, though material properties are commonly affected by smaller degrees of uncertainty. The nominal stiffness matrix of the four-node FE has $p_i = 5$ non-zero eigenvalues, as many as are the deformation modes of the element. The interval nodal displacements U_{jy}^I ($j = 1, 2, \ldots, 20$) and interval stress components $\sigma_{jy}^{(i)I}$ ($j = 1, 2, \ldots, 4$; $i = 1, 2, \ldots, N^{(e)}$) at the FE nodes, in the load direction are selected as response quantities of interest. The proposed bounds of the response are evaluated by applying both the *IRSE*-1 (see Section 4) and the *IRSE* truncated to second-order terms, which will be hereinafter referred to as *IRSE*-2. In the latter case, the sensitivity based procedure described in Section 5 is applied. The accuracy of the proposed IFEM is demonstrated by performing appropriate comparisons with the exact bounds of the response provided by the *vertex method* which requires 2^{16} deterministic analyses.

Figure 2 displays the comparison between the proposed and exact LB and UB of the interval nodal displacements U_{jy}^I ($j = 1, 2, \ldots, 20$) in the load direction evaluated for two different values of the deviation amplitude of the uncertain Young's moduli, say $\Delta\alpha = 0.1$ and $\Delta\alpha = 0.2$. Notice that the proposed bounds computed by applying the *IRSE*-1 are in good agreement with the exact ones even when the uncertainty level increases (see Figure 2b). Furthermore, as expected, when larger deviation amplitudes of the uncertain parameters are considered, the region containing all possible values of the response becomes wider.

To further assess the accuracy of the novel IFEM, in Figure 3 the absolute percentage errors, $\varepsilon_{\bar{U}_{jy}}(\%)$ and $\varepsilon_{\underline{U}_{jy}}(\%)$, affecting the proposed estimates of the bounds of the interval nodal displacements U_{jy}^{I} ($j = 1, 2, \ldots, 20$) obtained for $\Delta\alpha = 0.2$ by applying both the *IRSE*-1 and the *IRSE*-2 are reported. It is observed that the absolute percentage errors associated with the *IRSE*-1 are always less than 4% and thus acceptable from an engineering point of view. Furthermore, it can be seen that the *IRSE*-2, generally, yields a substantial improvement of the accuracy at the expense of a higher computational effort.

Both the proposed IFEM and the *vertex method* have been implemented in MATLAB and run on a PC with Intel® Core™ i7-2630QM CPU at 2.00 GHz and 4.00 GB RAM. The comparison between run-times has shown that the novel IFEM is much more efficient than the combinatorial procedure and its performance rapidly improves as the number of uncertain parameters increases. In particular, for the selected case study involving $N_e = 16$ uncertainties, the proposed IFEM based on the use of the *IRSE*-1 proves to be 324 times faster than the *vertex method*.

In order to quantify the propagation of Young's modulus uncertainty to the response of the plate, the so-called *coefficient of interval uncertainty* (c.i.u.)

$$\text{c.i.u.}[U_{jy}^{I}] = \frac{\Delta U_{jy}}{\left|\text{mid}\left\{U_{jy}^{I}\right\}\right|} = \frac{\bar{U}_{jy} - \underline{U}_{jy}}{\left|\bar{U}_{jy} + \underline{U}_{jy}\right|} \tag{55}$$

is evaluated. This coefficient provides a measure of the dispersion of the response around the midpoint value. Figure 4 shows the comparison between the *coefficient of interval uncertainty* of the nodal displacements U_{jy}^{I} ($j = 1, 2, \ldots, 20$) provided by the *IRSE*-1 and the exact one for two different degrees of uncertainty, say $\Delta\alpha = 0.1$ and $\Delta\alpha = 0.2$. As expected, the dispersion of the response around the midpoint value increases as larger deviation amplitudes of the uncertain Young's moduli are considered and is different for the various DOFs. In particular, it can be noticed that the displacements of the nodes lying on the free edges ($j = 1, 5, 6, 10, 11, 15, 16, 20$) are more affected by uncertainty than those of the inner nodes ($j = 2, 3, 4, 7, 8, 9, 12, 13, 14, 17, 18, 19$) located at the same distance from the fixed edge, with the largest dispersion over the whole plate pertaining to nodes 1 and 5. Furthermore, it is worth observing that the propagation of uncertainty implies an amplification for almost all DOFs. This result demonstrates the need of incorporating uncertainty in structural analysis in order to obtain reliable predictions of structural behavior.

Figure 5 and 6 display the LB and UB of the interval stress component in the load direction $\sigma_{jy}^{(i)I}$ ($j = 1, 2, \ldots, 4$; $i = 12, 16$) evaluated at the four nodes of FEs 12 and 16 (see Figure 1a), respectively, for $\Delta\alpha = 0.1$ and $\Delta\alpha = 0.2$. Notice that the proposed bounds, obtained by applying the *IRSE*-1, are in good agreement with the exact ones. The same level of accuracy is achieved for the bounds of the stress at the nodes of the remaining FEs, herein omitted for conciseness. To further scrutinize the accuracy of the novel IFEM, in Tables 1 and 2 the absolute percentage errors, $\varepsilon_{\bar{\sigma}_{jy}^{(i)}}(\%)$ and $\varepsilon_{\underline{\sigma}_{jy}^{(i)}}(\%)$, affecting the LB and UB of the interval stress component $\sigma_{jy}^{(i)I}$ ($j = 1, 2, \ldots, 4$; $i = 12, 16$) provided by both the *IRSE*-1 and *IRSE*-2 are listed. By inspection of these tables, it is inferred that the accuracy of the proposed IFEM does not worsen when stress variables are considered. Furthermore, it is observed that the *IRSE*-2, generally, allows a substantial reduction of the absolute percentage errors affecting the proposed estimates of stress bounds.

In order to investigate the influence of the FE mesh on the accuracy of the proposed IFEM, the plate under study is analyzed considering a uniform mesh consisting of $N_e = 64$ four-node 2D FEs. Since the *vertex method* requires 2^{64} deterministic analyses of the plate, the *SM* is applied for validation purpose. Furthermore, in order to compare the solutions pertaining to the two meshes with $N_e = 16$ and $N_e = 64$ FEs, the displacement components in the load direction of the nodes numbered in Figure 1a are considered as response quantities of interest, i.e. U_{jy}^I ($j = 1, 2, \ldots, 20$).

In Figure 7, the proposed bounds of the interval nodal displacements U_{jy}^I ($j = 1, 2, \ldots, 20$) produced by the *IRSE*-1 considering the refined mesh with $N_e = 64$ FEs are contrasted with those pertaining to the coarse mesh with $N_e = 16$ FEs for two different levels of uncertainty, say $\Delta\alpha = 0.1$ and $\Delta\alpha = 0.2$. Notice that the refined mesh yields a slightly wider region of the nodal displacements due to higher variability of Young's modulus. Similar comparisons on the stress bounds, omitted for conciseness, as expected, have shown a more appreciable influence of the mesh size. Figure 8 displays the absolute percentage errors, $\varepsilon_{\overline{U}_{jy}}(\%)$ and $\varepsilon_{\underline{U}_{jy}}(\%)$, affecting the proposed LB and UB of the interval nodal displacements U_{jy}^I ($j = 1, 2, \ldots, 20$) provided by the *IRSE*-1 compared to those given by the *SM* for $\Delta\alpha = 0.1$ and $\Delta\alpha = 0.2$. As expected, the accuracy worsens when the degree of uncertainty increases. Furthermore, it is observed that the percentage errors are comparable to those obtained for the coarse mesh with $N_e = 16$ FEs (see Figure 3). Based on these results, it may be concluded that the proposed IFEM is not affected by the overestimation of the solution range with the increase of the number of uncertain parameters which is a common drawback of interval-based methods.

7.1.2 Independent uncertain Young's moduli over selected regions

Let us assume now that the square plate under uniform traction is subdivided into four regions with independent interval Young's moduli, say $N_r = 4$ (see Figure 1b). Figure 9 displays the bounds of the interval nodal displacements U_{jy}^I ($j = 1, 2, \ldots, 20$) provided by the *IRSE*-1 for $\Delta\alpha = 0.1$ and two different FE meshes, that is $N_e = 16$ and $N_e = 64$. It can be observed that the bounds are less influenced by the FE mesh than those obtained assuming $N_r = N_e$ (see Figure 7) since the description of the spatial variability of uncertainty is kept unaltered ($N_r = 4$). Furthermore, the absolute percentage errors affecting the proposed bounds of displacements compared to those provided by the *vertex method*, herein omitted for conciseness, are less than 0.6% for both the meshes with $N_e = 16$ and $N_e = 64$. Finally, Figure 10 displays the comparison between the *coefficients of interval uncertainty* of the nodal displacements U_{jy}^I ($j = 1, 2, \ldots, 20$) provided by the *IRSE*-1 for $N_r = 4$ and $N_r = N_e$, considering also in this case two different FE meshes with $N_e = 16$ and $N_e = 64$. As expected, when $N_r = 4$ regions with uncertain Young's modulus are assumed, the dispersion of the response around the midpoint value is almost independent of the FE mesh. Conversely, when the same mesh is adopted to describe both the spatial variability of uncertainty and the behavior of the structure ($N_r = N_e$), the dispersion increases with the number of FEs and is obviously larger than that pertaining to the plate with $N_r = 4$ uncertain Young's moduli since $N_e > N_r$. Furthermore, when $N_r = 4$, consistently with the physical problem, the effects of uncertainty on the various DOFs are related to the node location, as if a sort of symmetry were restored, i.e. the displacements of the inner nodes ($j = 2,3,4,7,8,9,12,13,14,17,18,19$) exhibit almost the same dispersion which is lower than that of external node displacements ($j = 1,5,6,10,11,15,16,20$) at the same distance from the fixed edge. These results demonstrate the capability of the proposed IFEM to accurately predict the interval response whatever mesh is adopted to describe the spatial variability of the uncertain property. This remarkable feature is due to the use of the *EUI* which is kept linked to each uncertain parameter throughout the solution procedure.

7.2 Square plate with uncertain Young's modulus: load condition 2

Let us consider now the same square plate with uncertain Young's modulus analyzed in the previous section, subjected to the load condition 2 (LC2) shown in Figure 11, where $p = 20$ MPa. The analysis is carried out adopting a non-uniform mesh consisting of $N_e = 64$ four-node FEs (see Figure 11a). Two different meshes are considered for the uncertain material property: the first one coincides with the FE mesh ($N_r = N_e = 64$), so that each EF exhibits independent variations of Young's modulus (see Figure 11b); the second mesh consists of $N_r = 4$ regions with $E^{(j)}(\alpha_j^I) = E_0(1+\Delta\alpha_j \hat{e}_j^I)$, $(j = 1,2,3,4)$, as shown in Figure 11b. In both cases, the deviation amplitude of the uncertain parameters is set to $\Delta\alpha = 0.1$. Attention is focused on the interval displacements U_{jy}^I ($j = 1,2,\ldots,21$) of the nodes highlighted in Figure 11a. In order to apply the proposed procedure, the eigenvalues and eigenvectors of the nominal stiffness matrix of each FE with different dimensions are first evaluated.

Figure 12 displays the proposed bounds of the nodal displacements U_{jy}^I ($j = 1,2,\ldots,21$) computed by applying the *IRSE*-1 for the two uncertainty meshes $N_r = N_e = 64$ (Figure 12a) and $N_r = 4$ (Figure 12b) compared with the bounds provided by the *SM* and the *vertex method*, respectively. It can be observed that the proposed method yields accurate predictions of the interval response also when a non-uniform FE mesh is used. Indeed, the percentage errors affecting the proposed estimates of the displacement bounds, omitted for conciseness, are always less than 1.2% for $N_r = N_e = 64$ and 0.6% for $N_r = 4$.

The effect of the uncertainty mesh can be clearly detected by inspection of Figure 13 where the *coefficients of interval uncertainty* of the nodal displacements U_{jy}^I ($j = 1,2,\ldots,21$) provided by the *IRSE*-1 for $N_r = N_e = 64$ and $N_r = 4$ are reported. As expected, assuming independent variations of Young's modulus of each FE leads to higher dispersion of the response around the midpoint value than that pertaining to the plate with independent uncertainties over $N_r = 4$ regions. Indeed, in the latter case, each realization of the uncertain material property exhibits a smaller variability over the plate domain. Furthermore, as observed in the previous example, the uncertainty mesh with $N_r = 4$ regions leads to a sort of symmetry in the propagation of uncertainty since the displacements of the inner nodes ($j = 2,\ldots,6,9,,\ldots,13,16,\ldots,20$) exhibit the same dispersion which is smaller than that of the external nodes ($j = 1,7,8,14,15,21$) located at the same distance from the fixed edge.

7.3 3D cantilever beam with uncertain Young's modulus

The third example concerns a 3D cantilever beam with uncertain Young's modulus of the material (Figure 14) subjected to two point loads $F = 100$ kN at the free end. The beam has length $L = 5$ m and rectangular cross-section with width $b = 0.25$ m and thickness $h = 0.5$ m. The nominal Young's modulus and Poisson ratio of the material are selected as $E_0 = 20$ GPa and $\nu = 0.3$, respectively. The beam is discretized into $N_e = 320$ eight-node brick elements resulting in a FE model with 1800 DOFs. Young's modulus of each FE is modelled as an interval variable $E^{(i)}(\alpha_i^I) = E_0(1 + \Delta\alpha_i \hat{e}_i^I)$ with $\Delta\alpha_i = \Delta\alpha$, $i = 1,2,\ldots,N_e$. The number of non-zero eigenvalues of the nominal stiffness matrix of the eight-node brick FE is $p_i = 18$, as many as are the deformation modes of the element. The proposed IFEM is applied to evaluate the bounds of the interval displacement components, U_{jy}^I ($j = 1,2,\ldots,20$), along the y-axis of twenty selected nodes shown in Figure 14. The LB and UB of the interval stress component $\tau_{j\,xz}^{(165)I}$ ($j = 1,2,\ldots,8$) at the nodes of FE 165 highlighted in Figure 14 are also computed. The proposed approach based on the use of the *affine form* of the *IRSE*-1 (see Section 4) is applied for evaluating both displacement and stress bounds. Due to the large number of uncertain parameters involved ($N_e = 320$), the evaluation of the exact solution by means of the *vertex method* is unfeasible. Hence, the accuracy of the proposed method is assessed by comparison with the results provided by the *SM*.

In Figure 15, the proposed LB and UB of the selected nodal displacements, U^I_{jy} ($j=1,2,\ldots,20$), evaluated by applying the *IRSE*-1 for $\Delta\alpha = 0.1$ and $\Delta\alpha = 0.2$ are contrasted with the bounds provided by the *SM*. A very good agreement is observed even when the degree of uncertainty increases, despite the large number of uncertain parameters involved. As expected, the region of the interval displacements widens when larger deviation amplitudes of the uncertain parameters are considered. The absolute percentage errors affecting the proposed estimates of the displacement bounds for $\Delta\alpha = 0.1$ and $\Delta\alpha = 0.2$ when compared with those given by the *SM*, herein omitted for conciseness, are less than 1% and 4%, respectively, for all the selected DOFs.

Figure 16 displays the estimates of the *coefficient of interval uncertainty* of the selected nodal displacements provided by the *IRSE*-1 and the *SM* for two different degrees of uncertainty, say $\Delta\alpha = 0.1$ and $\Delta\alpha = 0.2$. It can be seen that the dispersion of the interval response of the cantilever beam around the midpoint value increases with the deviation amplitude of the uncertain parameters and involves amplification of input uncertainty for all the considered DOFs. In particular, the *coefficient of interval uncertainty* slightly increases moving towards the free end, with node 20 exhibiting the largest dispersion around the midpoint value.

Finally, in Figure 17 the LB and UB of the interval stress component $\tau^{(165)I}_{j\,xz}$ ($j=1,2,\ldots,8$) at the eight nodes of FE 165 (see Figure 14) for $\Delta\alpha = 0.1$ and $\Delta\alpha = 0.2$ are reported. The comparison between the proposed estimates obtained by applying the *IRSE*-1 and the *SM* solution shows a very good agreement even for $\Delta\alpha = 0.2$.

The presented numerical results demonstrate the capability of the proposed IFEM to handle a large number of uncertain parameters and accurately predict the bounds of both displacements and stresses even for a 3D FE model. In particular, it is worth emphasizing that for the selected examples, the *IRSE*-1 produces sufficiently accurate results for uncertainty levels ($\Delta\alpha = 0.2$) which are unlikely to be exceed in real engineering problems.

8. CONCLUSIONS

A novel Interval Finite Element Method (IFEM) for the static analysis of linear structures with uncertain parameters has been presented. The key idea of the method is to model the uncertain parameters as interval variables handled by means of the *improved interval analysis via extra unitary interval* (*IIA via EUI*), recently introduced in the literature to reduce the overestimation affecting the *classical interval analysis*. This approach associates a particular unitary interval, the so-called *EUI*, to each uncertain parameter thus enabling to keep track of dependencies between interval variables in both the assembly and solution stages of the finite element procedure. The bounds of the interval response in terms of displacements and stresses are derived in approximate closed-form by applying the so-called *Interval Rational Series Expansion* (*IRSE*) which provides an approximate explicit expression of the inverse of the interval stiffness matrix.

Numerical results concerning both 2D and 3D structures with uncertain Young's modulus of the material have been presented. The accuracy and efficiency of the presented procedure have been demonstrated by performing appropriate comparisons with the exact bounds of the response provided by a combinatorial method when feasible.

Some remarkable advantages of the novel IFEM are the following: *i*) the main steps are the same as those characterizing the standard FEM (i.e. derivation of element properties, assembly, solution and post-processing); *ii*) the lower bound and upper bound of the interval response are derived in approximate explicit form; *iii*) the method provides very accurate estimates of the bounds of both primary (displacements) and secondary (stresses) variables even for large degrees of uncertainty; *iv*) the accuracy is not affected by the mesh size; *v*) different meshes can be adopted to describe the behaviour of the structure and the spatial variability of the uncertain properties; *vi*) the analysis of large-size structures with several uncertain parameters can be handled.

The aforementioned features make the proposed IFEM a powerful tool to assess structural safety in the context of worst case analysis. Furthermore, the results provided by the IFEM are particularly valuable in early design stages when available data on the uncertain parameters are insufficient to justify a computationally intensive probabilistic analysis. Future developments will focus on the representation of the uncertain properties as interval fields in the context of the proposed IFEM based on the *IIA via EUI*.

Acknowledgments

The authors wish to express their gratitude to Prof. Giuseppe Muscolino for fruitful discussions. The authors also thank the two anonymous reviewers for their valuable suggestions.

REFERENCES

[1] B.M. Ayyub, G.J. Klir, Uncertainty modeling and analysis in engineering and the sciences. Chapman & Hall/CRC, Taylor & Francis Group, Boca Raton, 2006.

[2] D. Moens, D. Vandepitte, A survey of non-probabilistic uncertainty treatment in finite element analysis, Comput. Methods Appl. Mech. Eng. 194 (2005) 1527-1555.

[3] I. Elishakoff, M. Ohsaki, Optimization and anti-optimization of structures under uncertainty. Imperial College Press, London, 2010.

[4] A. Sofi, G. Muscolino, I. Elishakoff, Special section on nonprobabilistic approaches for handling uncertainty in engineering, ASCE-ASME J. Risk Uncertainty Eng. Syst., Part B: Mech. Eng. 1(3) (2015) 030201.

[5] A. Sofi, G. Muscolino, I. Elishakoff, Special issue on nonprobabilistic treatments of uncertainty: recent developments, ASCE-ASME J. Risk Uncertainty Eng. Syst., Part B: Mech. Eng. 1(4) (2015) 040301.

[6] R.B. Corotis, An overview of uncertainty concepts related to mechanical and civil engineering, ASCE-ASME J. Risk Uncertainty Eng. Syst., Part B: Mech. Eng. 1(4) (2015) 040801.

[7] R.E. Moore, Interval Analysis, Prentice-Hall, Englewood Cliffs, 1966.

[8] R.E. Moore, R.B. Kearfott, M.J. Cloud, Introduction to Interval Analysis, SIAM, Philadelphia, 2009.

[9] S.S. Rao, L. Berke, Analysis of uncertain structural systems using interval analysis, AIAA J 35(4) (1997) 727-735

[10] Z. Qiu, I. Elishakoff, Antioptimization of structures with large uncertain-but-non-random parameters via interval analysis, Comput. Methods Appl. Mech. Eng. 152 (1998) 361-372.

[11] S.H. Chen, H.D. Lian, X.W. Yang, Interval static displacement analysis for structures with interval parameters, Int. J. Numer. Meth. Eng. 53(2) (2002) 393–407.

[12] S. McWilliam, Anti-optimisation of uncertain structures using interval analysis, Comput. Struct. 79(4) (2001) 421–430.

[13] H.U. Köylüoğlu, I. Elishakoff, A comparison of stochastic and interval finite elements applied to shear frames with uncertain stiffness properties, Comput. Struct. 67 (1998)91-98.

[14] Z. Qiu, Y. Ma, X. Wang, Comparison between non-probabilistic interval analysis method and probabilistic approach in static response problem of structures with uncertain-but-bounded parameters, Commun. Numer. Meth. Eng. 20(4) (2004) 279–290.

[15] A. Pownuk Efficient method of solution of large scale engineering problems with interval parameters. In: Muhanna, RL, Mullen RL (eds), Proc. NSF Workshop on Reliable Engineering Computing, September 15–17, 2004, Savannah, Georgia, USA (2004) 305–316.

[16] D. Moens, M. Hanss, Non-probabilistic finite element analysis for parametric uncertainty treatment in applied mechanics: Recent advances, Finite Elem. Anal. Des. 47 (2011) 4-16.

[17] R.L. Muhanna, R.L. Mullen, Uncertainty in mechanics problems-interval-based approach, J. Eng. Mech. ASCE 127 (2001) 557-566.

[18] A. Neumaier, A. Pownuk, Linear systems with large uncertainties, with applications to truss structures, Reliab. Comput. 13(2) (2007) 149–172.

[19] J. Stolfi, L.H. De Figueiredo, An introduction to Affine Arithmetic, TEMA Tend. Mat. Apl. Comput. 4(3) (2003) 297-312.

[20] I. Elishakoff, Y. Miglis Novel parameterized intervals may lead to sharp bounds, Mech. Res. Commun. 44 (2012) 1-8.

[21] G. Muscolino, A. Sofi, Stochastic analysis of structures with uncertain-but-bounded parameters via improved interval analysis, Probab. Eng. Mech. 28 (2012) 152-163.

[22] D. Degrauwe, G. Lombaert, G. De Roeck, Improving interval analysis in finite element calculations by means of affine arithmetic, Comput. Struct. 88 (2010) 247–254.

[23] R. Santoro, G. Muscolino, I. Elishakoff, Optimization and anti-optimization solution of combined parameterized and improved interval analyses for structures with uncertainties, Comput. Struct. 149 (2015) 31–42.

[24] M.V. Rama Rao, R.L. Mullen, R.L. Muhanna, A new interval finite element formulation with the same accuracy in primary and derived variables, Int. J. Reliab. Safety 5(3) (2011) 336-357.

[25] R.L. Muhanna, H. Zhang, R.L. Mullen, Interval Finite Elements as a basis for generalized models of uncertainty in engineering mechanics. Reliab Comput 13 (2007) 173-194.

[26] R.L. Muhanna, H. Zhang, R.L. Mullen, Combined axial and bending stiffness in Interval Finite-Element Methods, J. Struct. Eng. ASCE 133(12) (2007) 1700-1709.

[27] N. Impollonia, G. Muscolino, Interval analysis of structures with uncertain-but-bounded axial stiffness, Comput. Methods Appl. Mech. Eng. 200 (21-22) (2011) 1945–1962.

[28] D. Moens, M. De Munck, W. Desmet, D. Vandepitte, Numerical dynamic analysis of uncertain mechanical structures based on interval fields, IUTAM Symposium on the Vibration Analysis of Structures with Uncertainties (A.K. Belyaev, R.S. Langley eds.) Springer, Dordrecht, 71-83; 2011.

[29] G. Muscolino, A. Sofi, M. Zingales, One-dimensional heterogeneous solids with uncertain elastic modulus in presence of long-range interactions: interval versus stochastic analysis, Comput Struct 122 (2013) 217-229.

[30] W. Verhaeghe, W. Desmet, D. Vandepitte, D. Moens, Interval fields to represent uncertainty on the output side of a static FE analysis, Comput Methods Appl Mech Eng 260 (2013) 50-62.

[31] C. Jiang, B.Y. Ni, X. Han, Y.R. Tao, Non-probabilistic convex model process: A new method of time-variant uncertainty analysis and its application to structural dynamic reliability problems, Comput. Methods Appl. Mech. Engrg. 268 (2014) 656–676.

[32] G. Muscolino, A. Sofi, Bounds for the stationary stochastic response of truss structures with uncertain-but-bounded parameters, Mech. Syst. Signal Pr. 37 (2013) 163-181.

[33] G. Muscolino, R. Santoro, A. Sofi, Explicit sensitivities of the response of discretized structures under stationary random processes, Probab. Eng. Mech. 35 (2014) 82-95.

[34] G. Muscolino, R. Santoro, A. Sofi, Explicit frequency response functions of discretized structures with uncertain parameters, Comput. Struct. 133 (2014) 64–78.

[35] G. Muscolino, R. Santoro, A. Sofi, Reliability analysis of structures with interval uncertainties under stationary stochastic excitations, Comput. Methods Appl. Mech. Engrg. 300 (2016) 47–69.

[36] J. Rohn, Interval solution of linear interval equations, Appl. Math. 35 (1990) 220-224.

[37] V. Kreinovich, J. Beck, C. Ferregut, A. Sanchez, G.R. Keller, M. Averill, S.A. Starks, Monte-Carlo-Type techniques for processing interval uncertainty, and their potential engineering applications. Reliab. Comput. 13 (2007) 25–69.

[38] W. Dong, H. Shah Vertex method for computing functions of fuzzy variables, Fuzzy Sets Syst. 24 (1987) 65–78.

FIGURE CAPTIONS

Figure 1. Square plate with uncertain Young's modulus under load condition 1 (LC1): a) FE mesh coincident with uncertainty mesh, i.e. $N_e = N_r$; b) alternative uncertainty mesh consisting of $N_r = 4$ regions.

Figure 2. LB and UB of the nodal displacements in the load direction of the plate (LC1) with uncertain Young's moduli $E^{(i)}(\alpha_i^I) = E_0^{(i)}\left(1+\Delta\alpha\,\hat{e}_i^I\right)$, $i=1,2,\ldots,16$, for a) $\Delta\alpha = 0.1$ and b) $\Delta\alpha = 0.2$: comparison between the proposed bounds obtained applying the *IRSE*-1 and the exact ones.

Figure 3. Absolute percentage errors affecting the proposed LB (a) and UB (b) of the nodal displacements in the load direction of the plate (LC1) with uncertain Young's moduli $E^{(i)}(\alpha_i^I) = E_0^{(i)}\left(1+\Delta\alpha\,\hat{e}_i^I\right)$, $i=1,2,\ldots,16$, obtained by applying the *IRSE*-1 and *IRSE*-2 ($\Delta\alpha = 0.2$).

Figure 4. *Coefficient of interval uncertainty* of the nodal displacements in the load direction of the plate (LC1) with uncertain Young's moduli $E^{(i)}(\alpha_i^I) = E_0^{(i)}\left(1+\Delta\alpha\,\hat{e}_i^I\right)$, $i=1,2,\ldots,16$: comparison between the exact and proposed estimates obtained by applying the *IRSE*-1 for $\Delta\alpha = 0.1$ and $\Delta\alpha = 0.2$.

Figure 5. LB and UB of the stress component in the load direction evaluated at the nodes of FE 12 of the plate (LC1) with uncertain Young's moduli $E^{(i)}(\alpha_i^I) = E_0^{(i)}\left(1+\Delta\alpha\,\hat{e}_i^I\right)$, $i=1,2,\ldots,16$, for a) $\Delta\alpha = 0.1$ and b) $\Delta\alpha = 0.2$: comparison between the proposed bounds obtained applying the *IRSE*-1 and the exact ones.

Figure 6. LB and UB of the stress component in the load direction evaluated at the nodes of FE 16 of the plate (LC1) with uncertain Young's moduli $E^{(i)}(\alpha_i^I) = E_0^{(i)}\left(1+\Delta\alpha\,\hat{e}_i^I\right)$, $i=1,2,\ldots,16$, for a) $\Delta\alpha = 0.1$ and b) $\Delta\alpha = 0.2$: comparison between the proposed bounds obtained applying the *IRSE*-1 and the exact ones.

Figure 7. Proposed LB and UB of the nodal displacements in the load direction of the plate (LC1) with uncertain Young's moduli $E^{(i)}(\alpha_i^I) = E_0^{(i)}\left(1+\Delta\alpha\,\hat{e}_i^I\right)$, $i=1,2,\ldots,N_e$, provided by the *IRSE*-1 for a) $\Delta\alpha = 0.1$ and b) $\Delta\alpha = 0.2$: comparison between the results pertaining to two different meshes with $N_e = 16$ and $N_e = 64$ FEs.

Figure 8. Absolute percentage errors affecting the proposed LB (a) and UB (b) of the nodal displacements in the load direction of the plate (LC1) with uncertain Young's moduli $E^{(i)}(\alpha_i^I) = E_0^{(i)}\left(1+\Delta\alpha\,\hat{e}_i^I\right)$, $i=1,2,\ldots,64$, obtained by applying the *IRSE*-1 for $\Delta\alpha = 0.1$ and $\Delta\alpha = 0.2$.

Figure 9. LB and UB of the nodal displacements in the load direction of the plate (LC1) with $N_r = 4$ regions with uncertain Young's moduli $E^{(i)}(\alpha_i^I) = E_0^{(i)}\left(1+\Delta\alpha\,\hat{e}_i^I\right)$, $i = 1,2,3,4$, ($\Delta\alpha = 0.1$): comparison between the estimates provided by the *IRSE*-1 for two different FE meshes with $N_e = 16$ and $N_e = 64$.

Figure 10. *Coefficient of interval uncertainty* of the nodal displacements in the load direction of the plate (LC1) with uncertain Young's moduli provided by the *IRSE*-1 for different FE (N_e) and uncertainty (N_r) meshes ($\Delta\alpha = 0.1$).

Figure 11. Square plate with uncertain Young's modulus under load condition 2 (LC2): a) FE mesh coincident with uncertainty mesh, i.e. $N_e = N_r$; b) alternative uncertainty mesh consisting of $N_r = 4$ regions.

Figure 12. LB and UB of the selected nodal displacements in the load direction of the plate (LC2) discretized into $N_e = 64$ FEs with a) $N_r = N_e = 64$ and b) $N_r = 4$ regions with uncertain Young's moduli: comparison between the estimates provided by the *IRSE*-1 and the bounds obtained applying the *SM* and the *vertex method*, respectively ($\Delta\alpha = 0.1$).

Figure 13. *Coefficient of interval uncertainty* of the selected nodal displacements in the load direction of the plate (LC2) discretized into $N_e = 64$ FEs provided by the *IRSE*-1 considering $N_r = N_e = 64$ and $N_r = 4$ regions with uncertain Young's moduli ($\Delta\alpha = 0.1$).

Figure 14. 3D cantilever beam with uncertain Young's modulus under two point loads.

Figure 15. LB and UB of twenty selected nodal displacements of the cantilever beam with uncertain Young's moduli $E^{(i)}(\alpha_i^I) = E_0^{(i)}\left(1+\Delta\alpha\,\hat{e}_i^I\right)$, $i = 1,2,\ldots,320$, for a) $\Delta\alpha = 0.1$ and b) $\Delta\alpha = 0.2$: comparison between the proposed bounds obtained applying the *IRSE*-1 and the ones provided by the *SM*.

Figure 16. *Coefficient of interval uncertainty* of twenty selected nodal displacements of the cantilever beam with uncertain Young's moduli $E^{(i)}(\alpha_i^I) = E_0^{(i)}\left(1+\Delta\alpha\,\hat{e}_i^I\right)$, $i = 1,2,\ldots,320$: comparison between the proposed estimates obtained by applying the *IRSE*-1 and the ones provided by the *SM* for $\Delta\alpha = 0.1$ and $\Delta\alpha = 0.2$.

Figure 17. LB and UB of the stress component $\tau_{j\,xz}^{(165)I}$ evaluated at the nodes of FE 165 of the cantilever beam with uncertain Young's moduli $E^{(i)}(\alpha_i^I) = E_0^{(i)}\left(1+\Delta\alpha\,\hat{e}_i^I\right)$, $i = 1,2,\ldots,320$, for: a) $\Delta\alpha = 0.1$ and b) $\Delta\alpha = 0.2$: comparison between the proposed bounds obtained applying the *IRSE*-1 and the ones provided by the *SM*.

Figure 18. Dr. Alba Sofi.

Figure 19. Eng. Eugenia Romeo.

TABLE CAPTIONS

Table 1. Absolute percentage errors affecting the proposed estimates of the bounds of the stress component in the load direction evaluated at the nodes of FE 12 of the plate (LC1) with uncertain Young's moduli $E^{(i)}(\alpha_i^I) = E_0^{(i)}\left(1+\Delta\alpha\,\hat{e}_i^I\right)$, $i=1,2,\ldots,16$, by applying the *IRSE*-1 and *IRSE*-2 ($\Delta\alpha = 0.2$).

Table 2. Absolute percentage errors affecting the proposed estimates of the bounds of the stress component in the load direction evaluated at the nodes of FE 16 of the plate (LC1) with uncertain Young's moduli $E^{(i)}(\alpha_i^I) = E_0^{(i)}\left(1+\Delta\alpha\,\hat{e}_i^I\right)$, $i=1,2,\ldots,16$, by applying the *IRSE*-1 and *IRSE*-2 ($\Delta\alpha = 0.2$).

SHORT BIOGRAPHIES OF THE AUTHORS

Alba Sofi is Assistant Professor of Structural Mechanics at University “Mediterranea” of Reggio Calabria (Italy). She received her Ph.D degree in Structural Engineering from the University of Palermo (Italy) in 2002. In 2004, she was appointed as Visiting Scholar at Rice University (Houston, USA). In 2016 she was appointed as Visiting Fellow at the Department of Engineering Science, University of Oxford (UK). She is active referee for several International Journals. She serves as Member of the Editorial Board of the *ASCE-ASME Journal of Risk and Uncertainty in Engineering Systems*. Her primary research interests focus on: stochastic dynamics; probabilistic and non-probabilistic approaches in uncertainty quantification with specific expertise in interval analysis; bridge-vehicle dynamic interaction; cable dynamics; non-local elasticity theory.

Eugenia Romeo received her Master of Science degree in Civil Engineering cum Laude and academic mention from the University “Mediterranea” of Reggio Calabria (Italy) in 2014. She is specialized in “Structural, Infrastructural and Geotechnical Design”. Currently, she is working as a Ph.D student on a project concerning uncertainty propagation in finite element modeled structures. In June 2015, she has been awarded with a scholarship for the research project entitled “Hy_Compo_2020, Hybridized Composite and Powertrain system for Europe 2020”, at University “Federico II” of Naples (Italy).

FIGURE 1

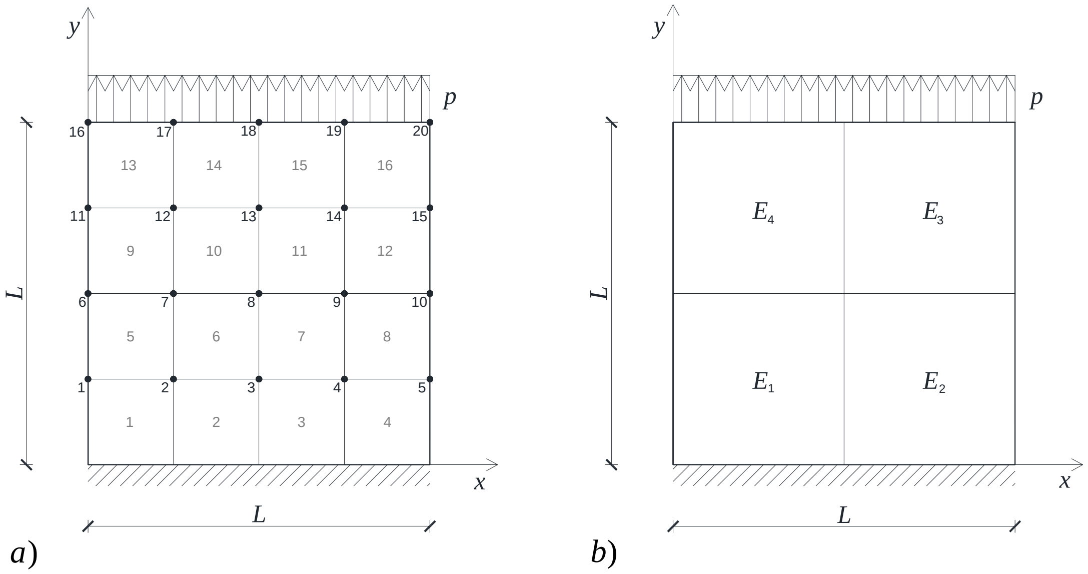

Figure 1. Square plate with uncertain Young's modulus under load condition 1 (LC1): a) FE mesh coincident with uncertainty mesh, i.e. $N_e = N_r$; b) alternative uncertainty mesh consisting of $N_r = 4$ regions.

FIGURE 2

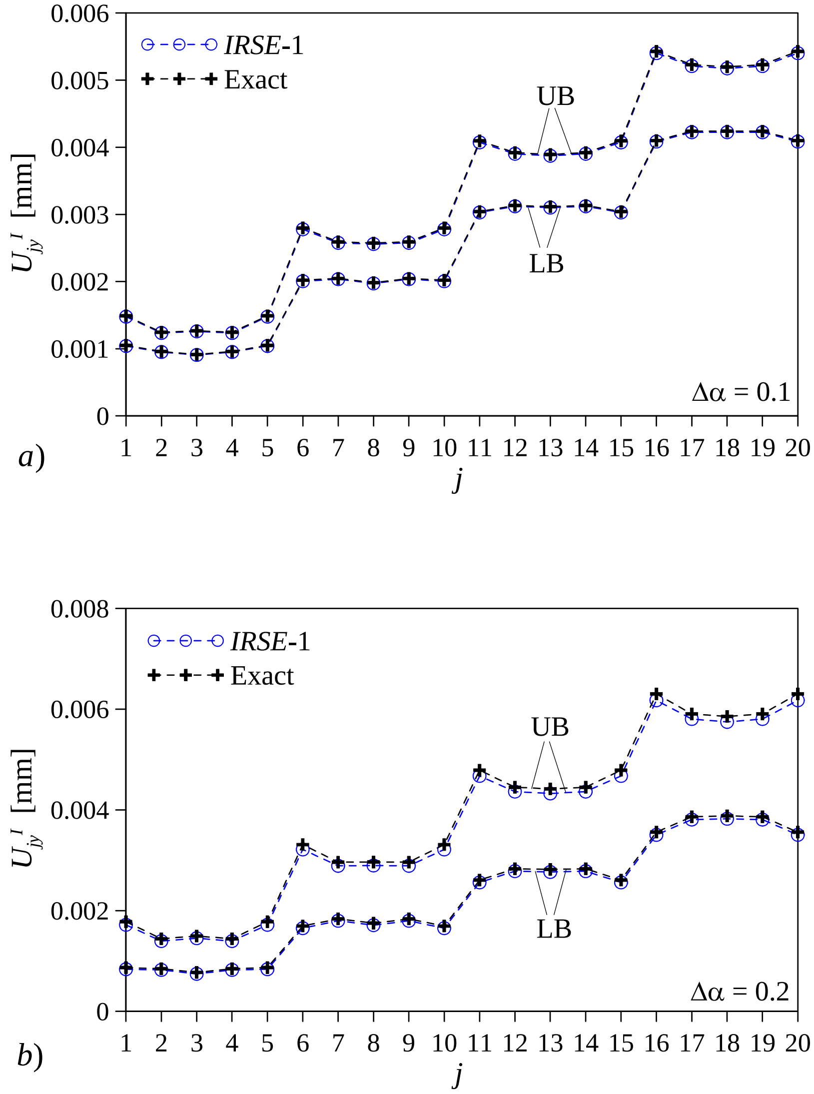

Figure 2. LB and UB of the nodal displacements in the load direction of the plate (LC1) with uncertain Young's moduli $E^{(i)}(\alpha_i^I) = E_0^{(i)}\left(1+\Delta\alpha\,\hat{e}_i^I\right)$, $i = 1, 2, \ldots, 16$, for a) $\Delta\alpha = 0.1$ and b) $\Delta\alpha = 0.2$: comparison between the proposed bounds obtained applying the *IRSE*-1 and the exact ones.

FIGURE 3

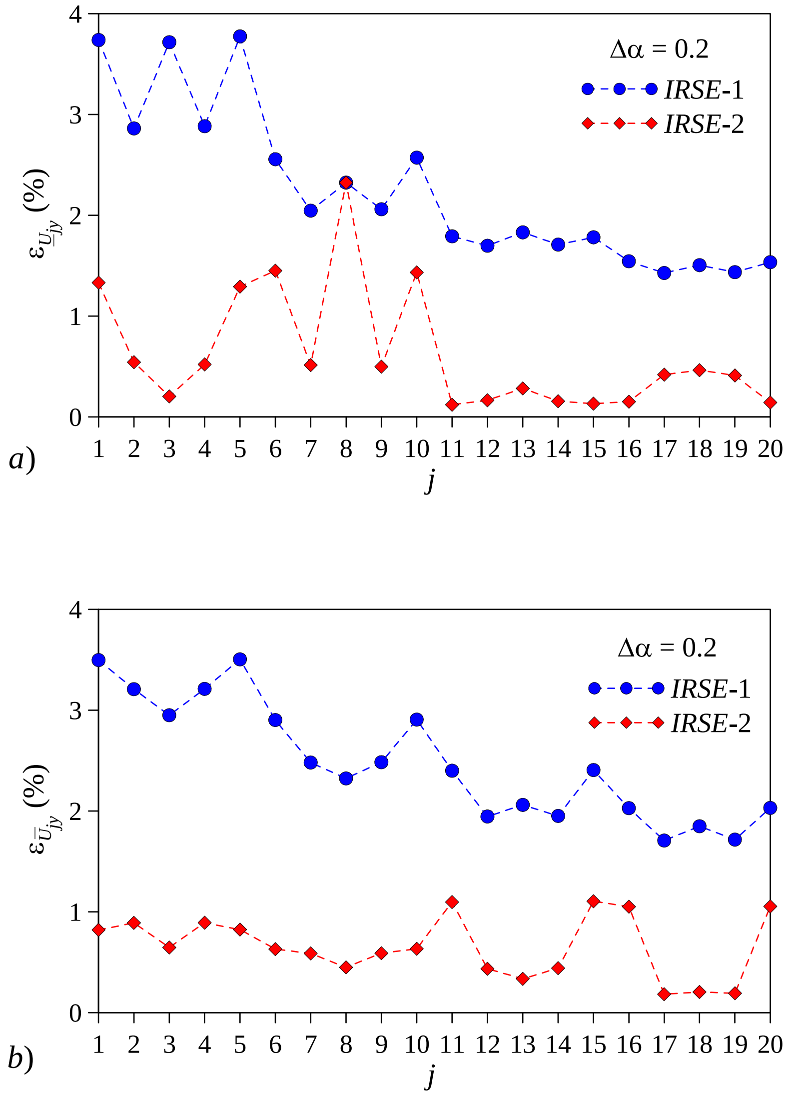

Figure 3. Absolute percentage errors affecting the proposed LB (a) and UB (b) of the nodal displacements in the load direction of the plate (LC1) with uncertain Young's moduli $E^{(i)}(\alpha_i^I) = E_0^{(i)}\left(1+\Delta\alpha\,\hat{e}_i^I\right)$, $i = 1, 2, \ldots, 16$, obtained by applying the *IRSE*-1 and *IRSE*-2 ($\Delta\alpha = 0.2$).

FIGURE 4

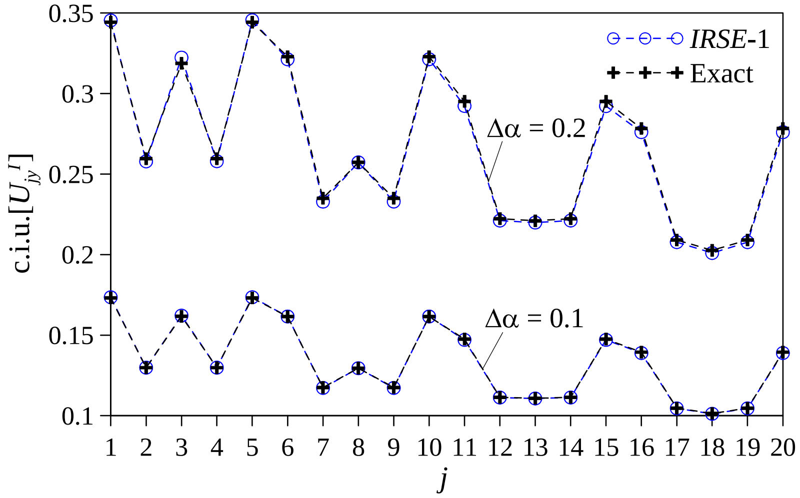

Figure 4. *Coefficient of interval uncertainty* of the nodal displacements in the load direction of the plate (LC1) with uncertain Young's moduli $E^{(i)}(\alpha_i^I) = E_0^{(i)}\left(1+\Delta\alpha\,\hat{e}_i^I\right)$, $i=1,2,\ldots,16$: comparison between the exact and proposed estimates obtained by applying the *IRSE*-1 for $\Delta\alpha = 0.1$ and $\Delta\alpha = 0.2$.

FIGURE 5

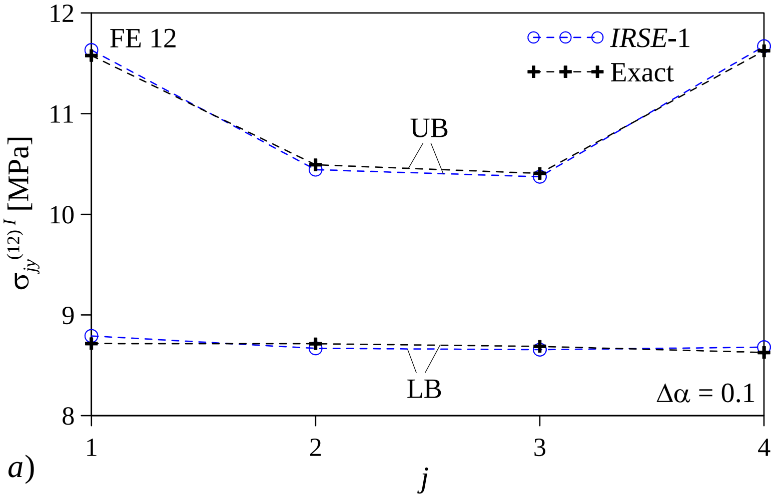

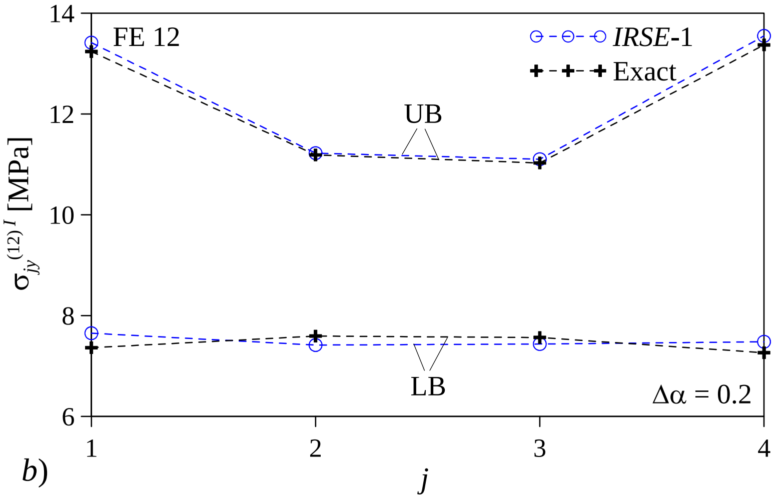

Figure 5. LB and UB of the stress component in the load direction evaluated at the nodes of FE 12 of the plate (LC1) with uncertain Young's moduli $E^{(i)}(\alpha_i^I) = E_0^{(i)}\left(1+\Delta\alpha\,\hat{e}_i^I\right)$, $i = 1,2,\ldots,16$, for a) $\Delta\alpha = 0.1$ and b) $\Delta\alpha = 0.2$: comparison between the proposed bounds obtained applying the *IRSE*-1 and the exact ones.

FIGURE 6

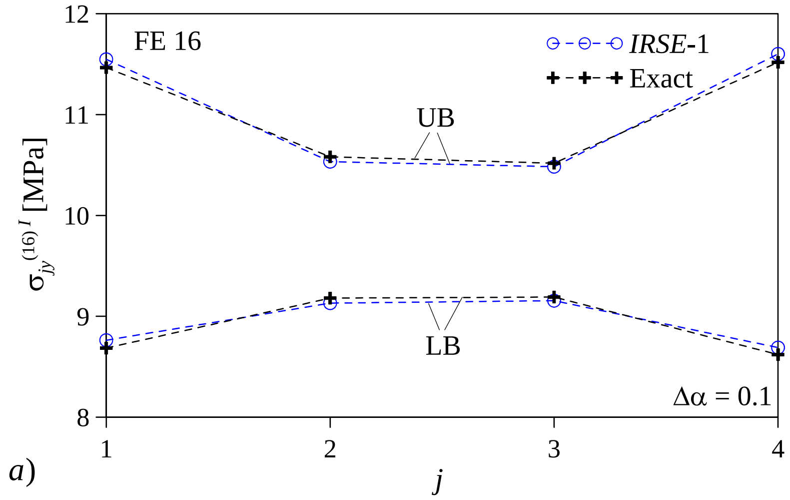

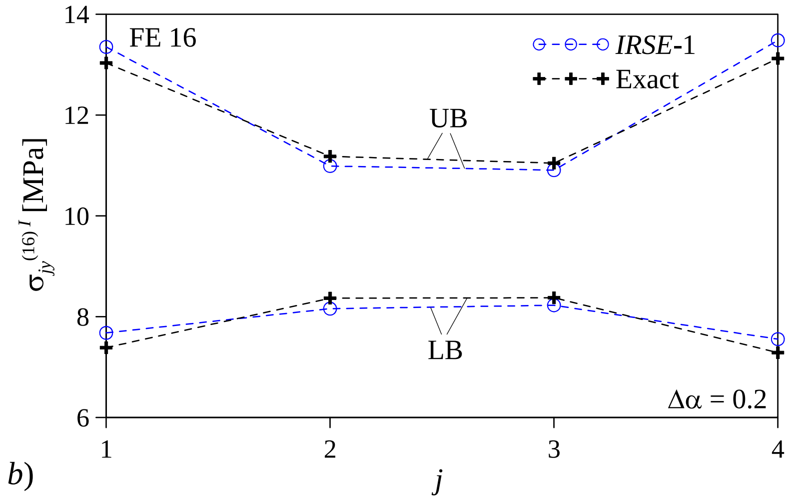

Figure 6. LB and UB of the stress component in the load direction evaluated at the nodes of FE 16 of the plate (LC1) with uncertain Young's moduli $E^{(i)}(\alpha_i^I) = E_0^{(i)}\left(1+\Delta\alpha\,\hat{e}_i^I\right)$, $i=1,2,\ldots,16$, for a) $\Delta\alpha = 0.1$ and b) $\Delta\alpha = 0.2$: comparison between the proposed bounds obtained applying the *IRSE*-1 and the exact ones.

FIGURE 7

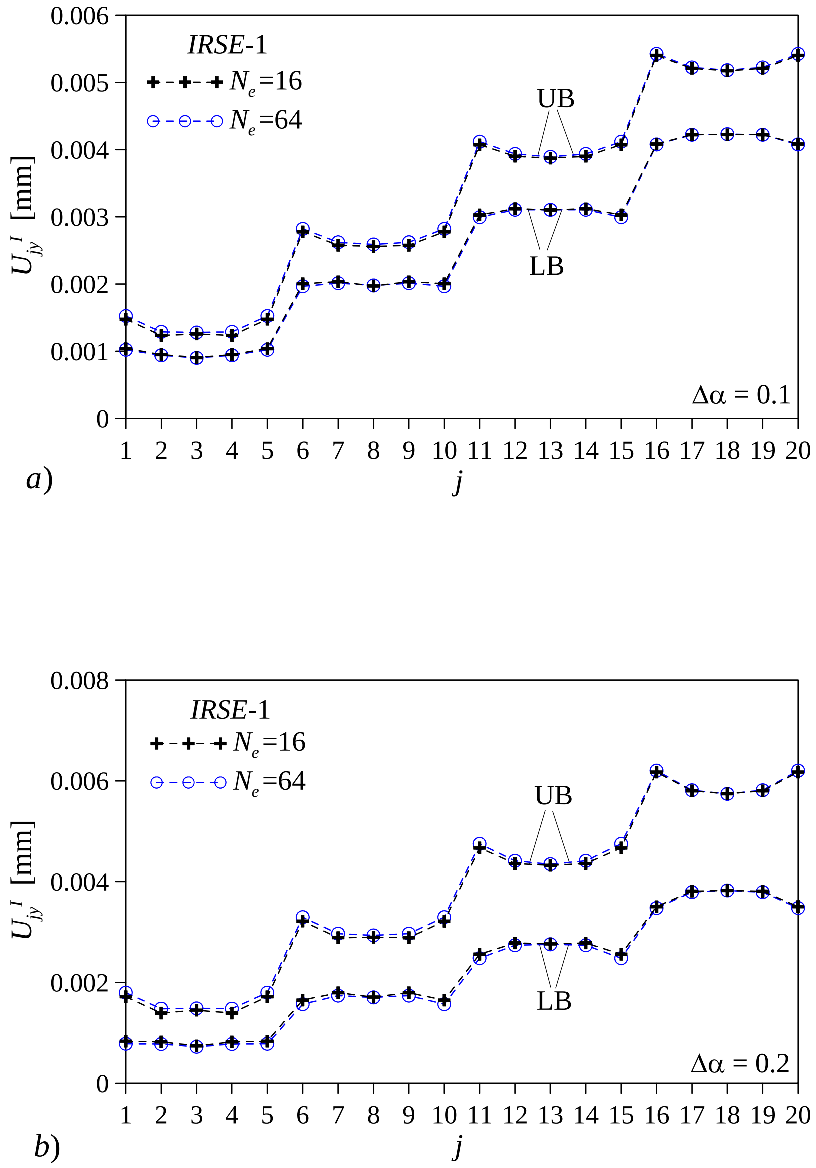

Figure 7. Proposed LB and UB of the nodal displacements in the load direction of the plate (LC1) with uncertain Young's moduli $E^{(i)}(\alpha_i^I) = E_0^{(i)}\left(1+\Delta\alpha\,\hat{e}_i^I\right)$, $i=1,2,\ldots,N_e$, provided by the *IRSE*-1 for a) $\Delta\alpha = 0.1$ and b) $\Delta\alpha = 0.2$: comparison between the results pertaining to two different meshes with $N_e = 16$ and $N_e = 64$ FEs.

FIGURE 8

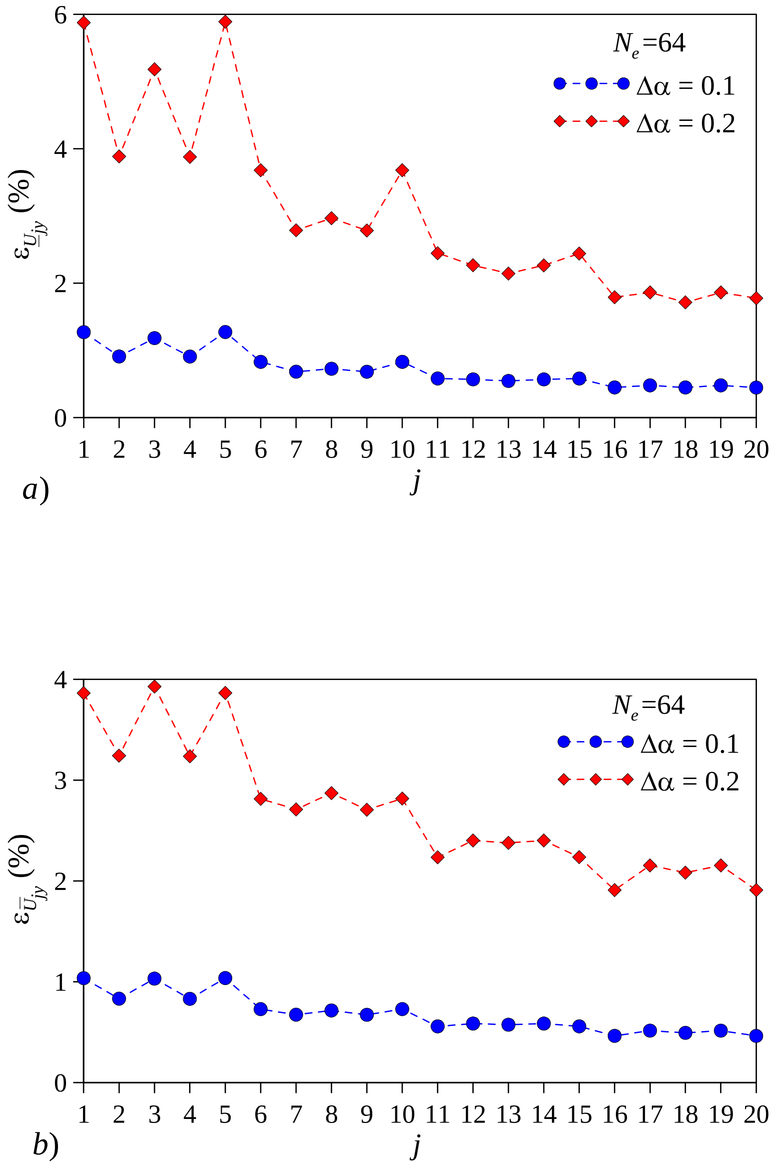

Figure 8. Absolute percentage errors affecting the proposed LB (a) and UB (b) of the nodal displacements in the load direction of the plate (LC1) with uncertain Young's moduli $E^{(i)}(\alpha_i^I) = E_0^{(i)}\left(1+\Delta\alpha\,\hat{e}_i^I\right)$, $i=1,2,\ldots,64$, obtained by applying the *IRSE*-1 for $\Delta\alpha = 0.1$ and $\Delta\alpha = 0.2$.

FIGURE 9

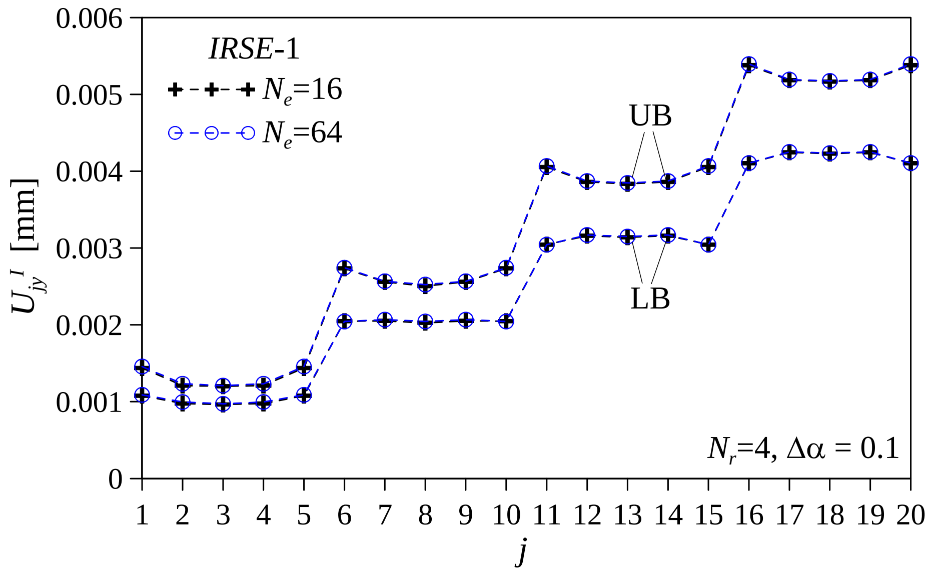

Figure 9. LB and UB of the nodal displacements in the load direction of the plate (LC1) with $N_r = 4$ regions with uncertain Young's moduli $E^{(i)}(\alpha_i^I) = E_0^{(i)}\left(1 + \Delta\alpha\,\hat{e}_i^I\right)$, $i = 1, 2, 3, 4$, ($\Delta\alpha = 0.1$): comparison between the estimates provided by the *IRSE*-1 for two different FE meshes with $N_e = 16$ and $N_e = 64$.

FIGURE 10

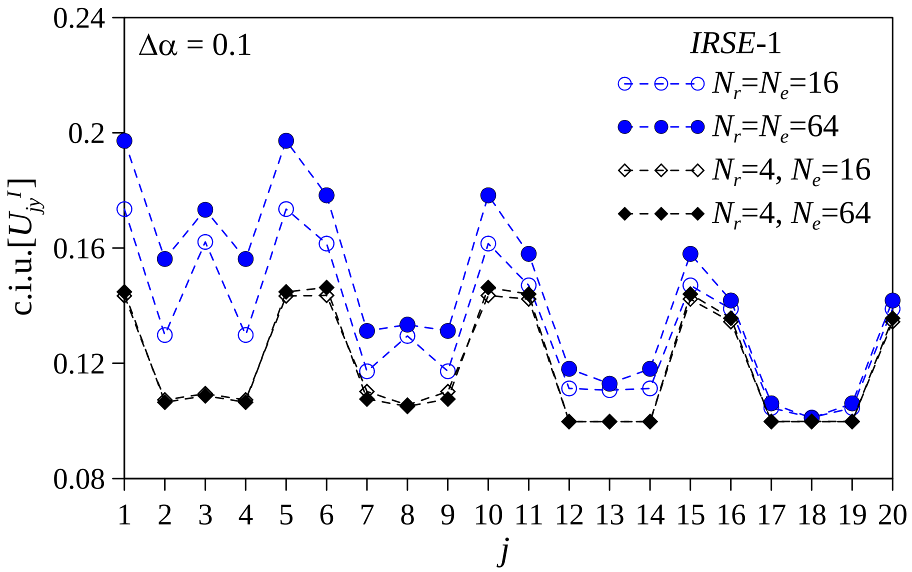

Figure 10. *Coefficient of interval uncertainty* of the nodal displacements in the load direction of the plate (LC1) with uncertain Young's moduli provided by the *IRSE*-1 for different FE (N_e) and uncertainty (N_r) meshes ($\Delta\alpha = 0.1$).

FIGURE 11

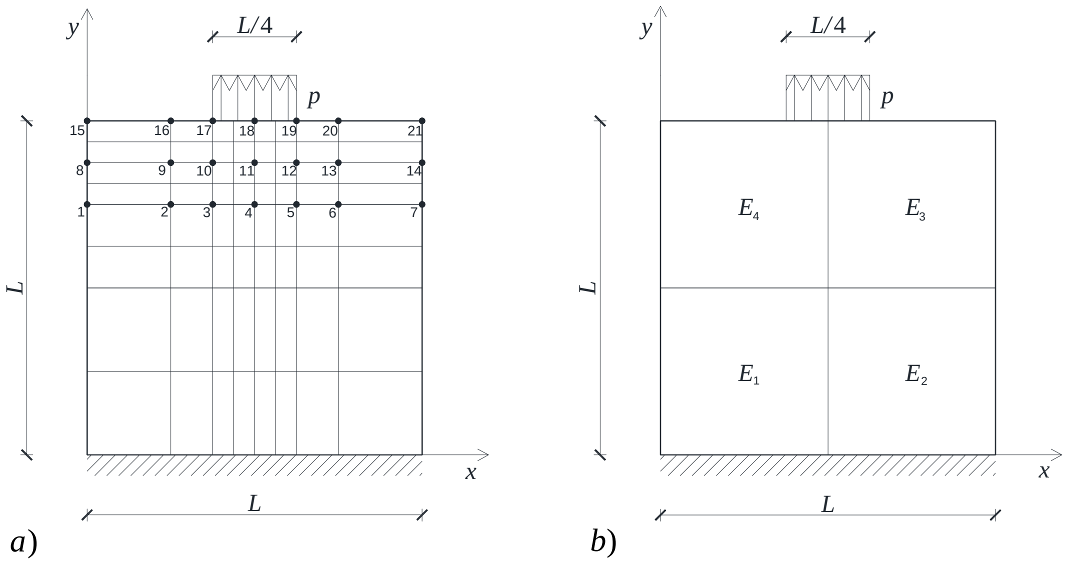

Figure 11. Square plate with uncertain Young's modulus under load condition 2 (LC2): a) FE mesh coincident with uncertainty mesh, i.e. $N_e = N_r$; b) alternative uncertainty mesh consisting of $N_r = 4$ regions.

FIGURE 12

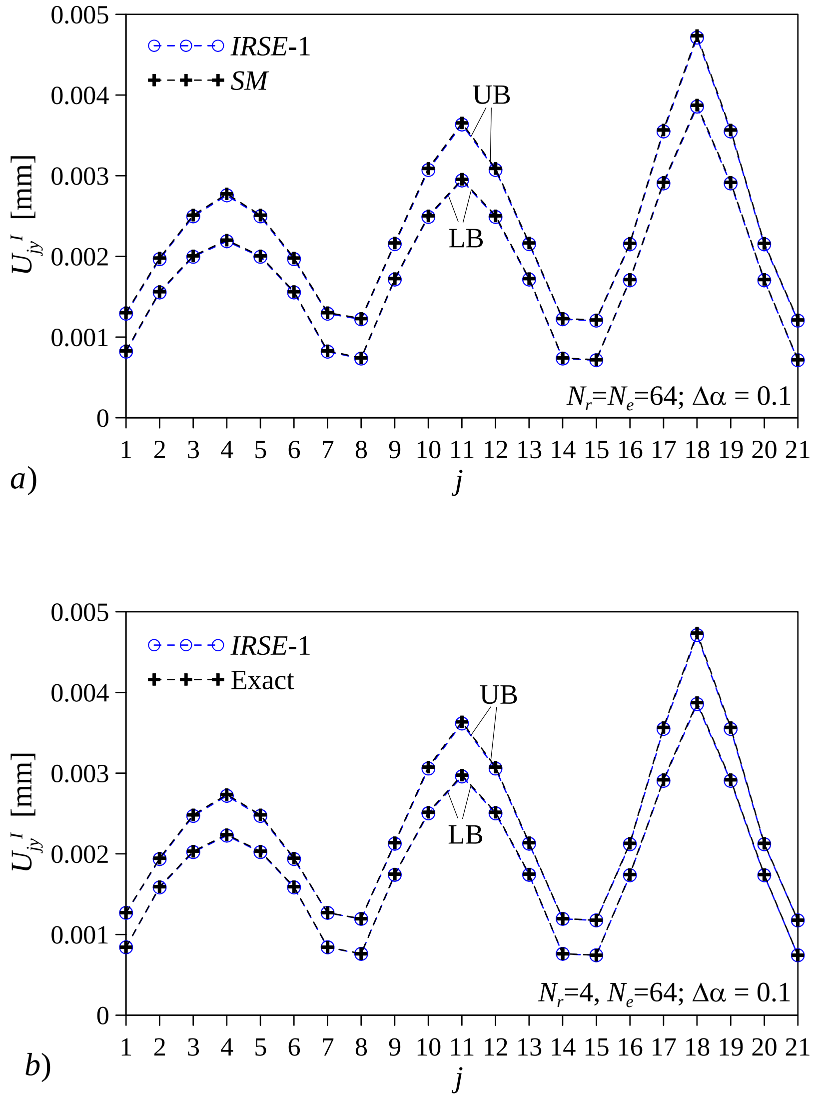

Figure 12. LB and UB of the selected nodal displacements in the load direction of the plate (LC2) discretized into $N_e = 64$ FEs with a) $N_r = N_e = 64$ and b) $N_r = 4$ regions with uncertain Young's moduli: comparison between the estimates provided by the *IRSE*-1 and the bounds obtained applying the *SM* and the *vertex method*, respectively ($\Delta\alpha = 0.1$).

FIGURE 13

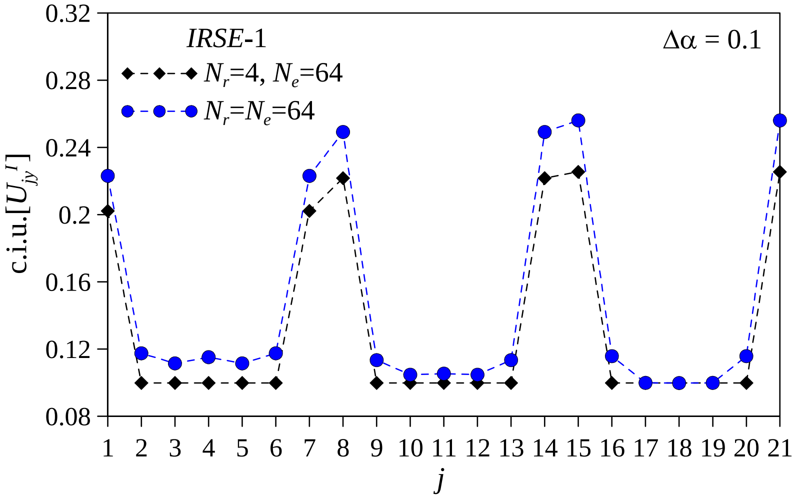

Figure 13. *Coefficient of interval uncertainty* of the selected nodal displacements in the load direction of the plate (LC2) discretized into $N_e = 64$ FEs provided by the *IRSE*-1 considering $N_r = N_e = 64$ and $N_r = 4$ regions with uncertain Young's moduli ($\Delta\alpha = 0.1$).

FIGURE 14

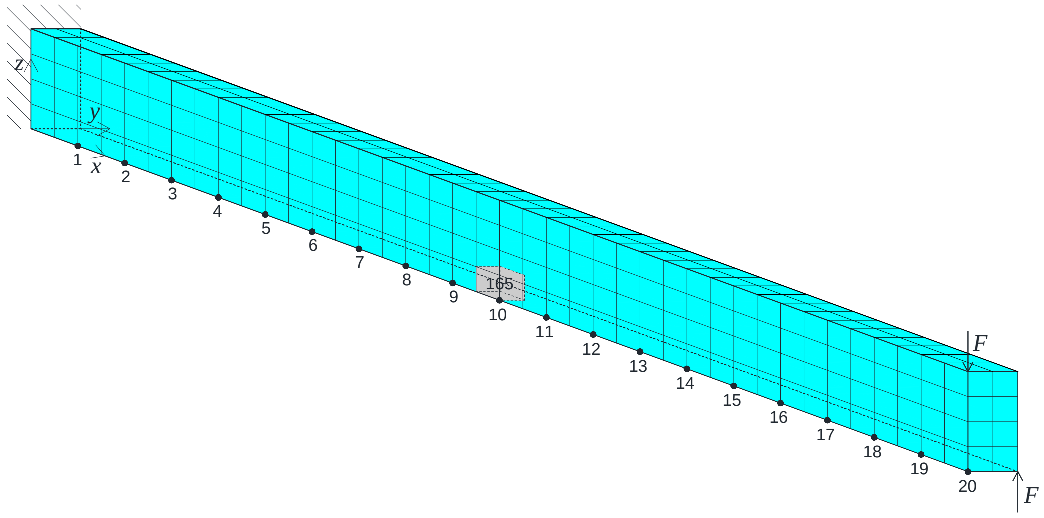

Figure 14. 3D cantilever beam with uncertain Young’s modulus under two point loads.

FIGURE 15

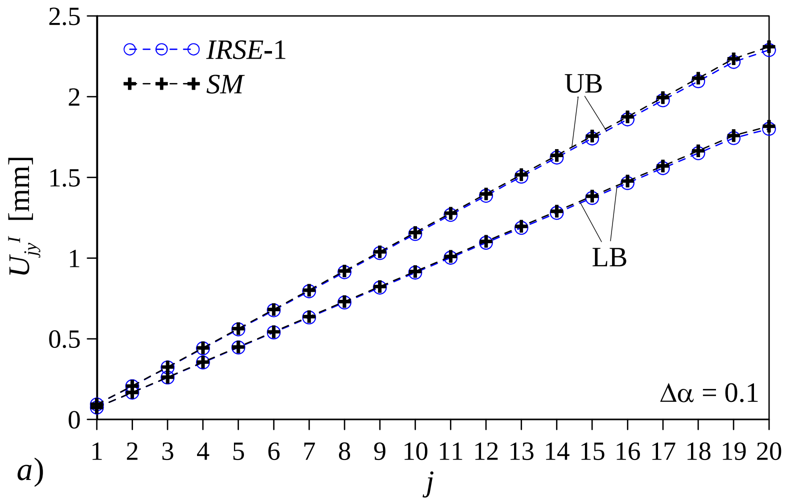

a)

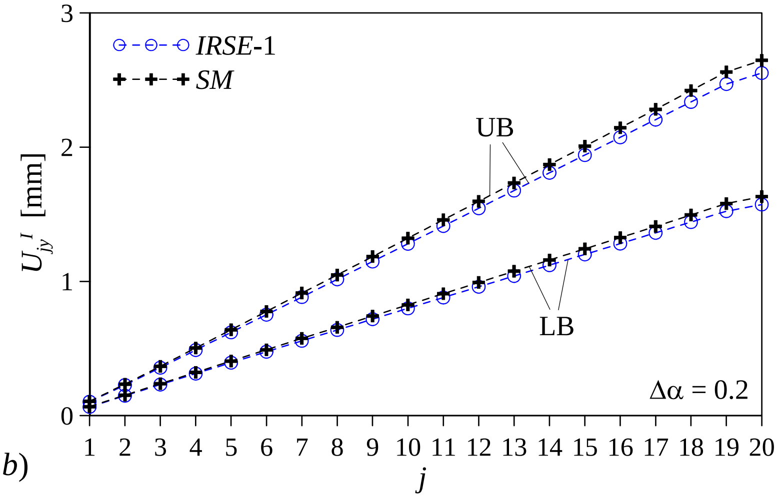

b)

Figure 15. LB and UB of twenty selected nodal displacements of the cantilever beam with uncertain Young's moduli $E^{(i)}(\alpha_i^I) = E_0^{(i)}\left(1 + \Delta\alpha\,\hat{e}_i^I\right)$, $i = 1, 2, \ldots, 320$, for a) $\Delta\alpha = 0.1$ and b) $\Delta\alpha = 0.2$: comparison between the proposed bounds obtained applying the *IRSE*-1 and the ones provided by the *SM*.

FIGURE 16

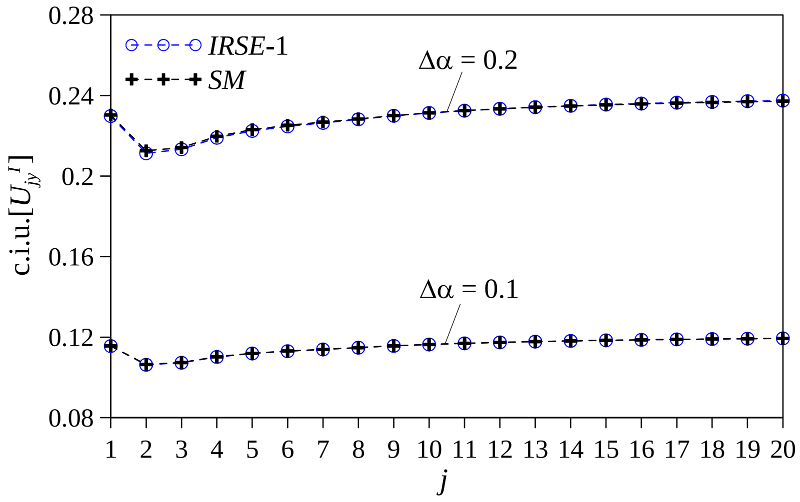

Figure 16. *Coefficient of interval uncertainty* of twenty selected nodal displacements of the cantilever beam with uncertain Young's moduli $E^{(i)}(\alpha_i^I) = E_0^{(i)}\left(1+\Delta\alpha\,\hat{e}_i^I\right)$, $i = 1, 2, \ldots, 320$: comparison between the proposed estimates obtained by applying the *IRSE*-1 and the ones provided by the *SM* for $\Delta\alpha = 0.1$ and $\Delta\alpha = 0.2$.

FIGURE 17

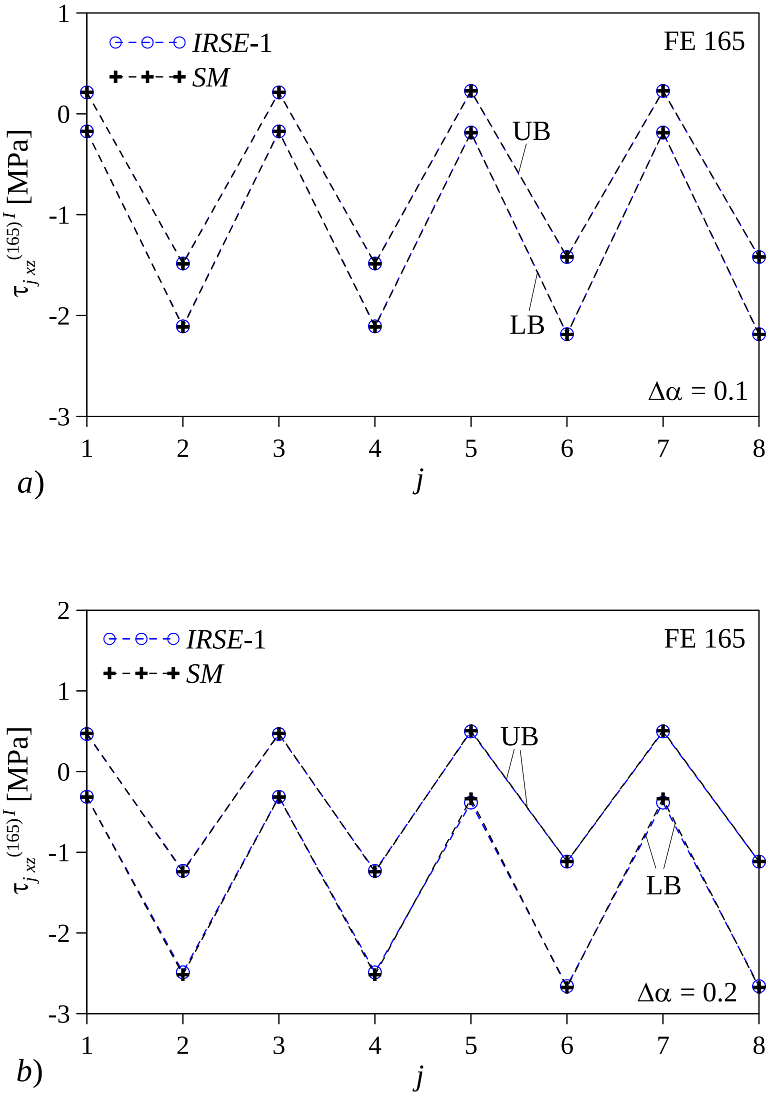

Figure 17. LB and UB of the stress component $\tau_{j\,xz}^{(165)I}$ evaluated at the nodes of FE 165 of the cantilever beam with uncertain Young's moduli $E^{(i)}(\alpha_i^I) = E_0^{(i)}\left(1+\Delta\alpha\,\hat{e}_i^I\right)$, $i=1,2,\ldots,320$, for: a) $\Delta\alpha = 0.1$ and b) $\Delta\alpha = 0.2$: comparison between the proposed bounds obtained applying the *IRSE*-1 and the ones provided by the *SM*.

FIGURE 18

Figure 18. Dr. Alba Sofi

FIGURE 19

Figure 19. Eng. Eugenia Romeo